International Journal of Solids and Structures 301 (2024) 112970

Contents lists available at ScienceDirect

International Journal of Solids and Structures

journal homepage: www.elsevier.com/locate/ijsolstr

Crack layer modeling of butt-fusion joints induced slow crack growth in high-density polyethylene pipes

Abdulla Almomani [a], Abdel-Hamid I. Mourad [a,b,c,*]

[a] Department of Mechanical and Aerospace Engineering, United Arab Emirates University, Al-Ain P.O. Box 15551, United Arab Emirates
[b] National Water and Energy Center, United Arab Emirates University, Al Ain P.O Box 15551, United Arab Emirates
[c] On leave from Mechanical Design Department, Faculty of Engineering, Helwan University, Cairo, El Mataria P.O. Box 11718, Egypt

ARTICLE INFO

Keywords:
Crack layer theory
Slow crack growth
High density polyethylene
Pipes
Butt-fusion joint
Lifetime prediction

ABSTRACT

The design and reliability of high-density polyethylene (HDPE) pipes can be dictated by the damage tolerance of their butt-fusion joints. A slow crack growth (SCG) model based on the crack layer theory for HDPE pipes internal and external circumferential and butt-fusion joints cracks is developed to investigate the discontinuous SCG behavior and lifetime t_f variations. Using the developed model, the discontinuous SCG patterns, jump lengths and lifetime t_f can be accurately simulated. In addition, the effects of pipes standard dimension ratio, internal pressure, and temperature on the SCG behavior and t_f are investigated. Compared to pipe cracks, it was found that butt-fusion induced SCG can reduce the pipe $t_f > 60$ %. Unlike longitudinal cracks, t_f of external circumferential cracks, were found shorter than the internal ones, mandating an earlier evaluation. The new SCG model shows good accuracy with the experimental results. The same substitute geometry approach used can be followed for other complex designs, which aids in establishing a fundamental methodology for more realistic lifetime predictions.

1. Introduction

The integrity of pressurized high-density polyethylene (HDPE) pipes requires careful assessment given the material unique crack and plastic zone interplay (Almomani et al., 2022; Benhamena et al., 2011; Benhamena et al., 2010; Deblieck et al., 2011; Favier et al., 2002; Plummer et al., 2001), and their critical applications in nuclear and oil and gas networks (Almomani et al., 2023; Hutař et al., 2011; Nasiri & Khosravani, 2023; Shi et al., 2023). The strength and longevity of an HDPE pipe can largely be dictated by the damage tolerance of their joints, i.e., butt-fusion welds (El-Bagory et al., 2021; Kim et al., 2019; Lee et al., 2022; Lu et al., 1992). Although the procedure of welding is standardized, geometrical heterogenies such as non-uniform bead profiles, misalignment offsets, or sharp notches in between the beads, as illustrated in Fig. 1(a-c), can be crack initiation sites and control the life expectancy of the bulk pipe (Bowman & Parmar, 1989; Carpinteri et al., 2003; Mikula et al., 2015; Mourad et al., 2013). Further, depending on the applied hoop stress and environmental conditions, HDPE can exhibit different modes of failure (Byrne et al., 2023; Mourad et al., 2003; Schoeffl & Lang, 2015). For example, at high hoop stresses delayed necking can lead to ductile failures (Krishnaswamy & Lamborn, 2005; Soltaninezhad et al., 2019), while intermediate loads can develop quasi-brittle slow crack growth (SCG) (Mourad & Maiti, 1995; Schouwenaars et al., 2007), and low stresses can form chemical degradation induced cracks (Barton et al., 2019; Chudnovsky et al., 2012; Lancioni et al., 2023; Wang et al., 2023). Among all, SCG being a well reproducible process and the most frequently observed mode in field failures facilitates modeling and consequently lifetime predictions (Maiti & Mourad, 1995b; Mourad & Maiti, 1996; Trávníček et al., 2023; Zha et al., 2022).

The formation of the process zone (PZ) in HDPE ahead of the crack, as shown in Fig. 1(d-f), can still result in a complex SCG behavior of continuous and discontinuous modes (Balika et al., 2007; Chudnovsky, 2014; Parsons et al., 2000). Due to the change in kinetics over time from the transition in the SCG modes, extrapolations of experimental data can be ineffective (Chudnovsky et al., 2012). At the same time, several test methods have been standardized to evaluate the SCG resistance of polyethylene (PE) (Nguyen et al., 2021). This includes ones for manufactured pipes such as the notched pipe test (NPT) (ISO, 2009) and the notched ring test (NRT) (Allwood & Beech, 1993; ISO, 2012; Laiarinandrasana et al., 2011). Also, ones favored for resin testing such as the Pennsylvania edge notched test (PENT) (ISO, 2005), and full notched creep test (FNCT) (ISO, 2019; Nezbedová et al., 2013; Thuy et al., 2021). The advancement of PE resin's performance, e.g., multimodal PE grades,

* Corresponding author at: Department of Mechanical and Aerospace Engineering, United Arab Emirates University, Al-Ain P.O. Box 15551, United Arab Emirates.
E-mail address: ahmourad@uaeu.ac.ae (A.-H.I. Mourad).

https://doi.org/10.1016/j.ijsolstr.2024.112970
Received 28 March 2024; Received in revised form 24 June 2024; Accepted 8 July 2024
Available online 9 July 2024

Nomenclature

Acronyms

AZ	Active zone
CL	Crack layer
COD	Crack opening displacement
DB	Dugdale–Barenblatt
ERR	Energy release rate
FEA	Finite element analysis
HDPE	High density polyethylene
MFZ	Melt flow zone
NPT	Notched pipe test
NRT	Notched ring test
SCG	Slow crack growth
SDR	Standard dimension ratio
SENT	Singe edge notched tension
SIF	Stress intensity factor
SFE	Specific fracture energy
TF	Thermodynamic force
PZ	Process zone
WZ	Wake zone
WE	Weld edge
WC	Weld center

List of Symbols

K	Stress intensity factor
K_{Ic}	Mode I critical stress intensity factor
k_{CR}, k_{PZ}	Crack and process zone kinetic coefficients
l_{CR}, l_{PZ}	Crack length and process zone length
L	Crack layer length
P_i	Internal pressure of the pipe
R_o, R_i	Outer and inner radius of pipe
G_{tot}	Total Gibbs potential energy
G^{SIF}, G^{COD}	Green function for stress intensity factor and crack opening displacement
t_f	Time to failure
σ_z	Resultant axial stress
σ_θ	Resultant hoop stress
σ_{dr}	Drawing stress
σ_b	Boundary traction stress
δ_{tot}	Crack opening displacement
λ	Natural drawing ratio
a	Crack length of elastic body
A, m, n	Material parameters
W	Crack line width
X^{CR}, X^{PZ}	Crack and process zone corresponding driving forces
l^{CR}	Length of the crack
J_1^{CR}, J_1^{PZ}	The Energy release rate for the crack and process zone
R_I	Volumetric quantity of transformed material to PZ
E'	The elastic modulus
2γ	Specific fracture energy
$2\gamma_0$	Initial specific fracture energy of fresh material
γ^{tr}	Transformation energy per unit volume
β_n	Coefficients for Green's function for stress intensity factor
μ_i	Coefficients for correction factor

and the excessive testing times have led to the development of novel accelerated testing methods using pulsation techniques and wetting agents such as the crack round bar (CRB) (ISO, 2015) and accelerated notched pipe test (aNPT) (Fischer et al., 2019; Robledo et al., 2017). Yet, such methods fail to deliver a comprehensive SCG test method and suffer from asymmetric crack growth that can be driven by load line misalignments, eccentric initial notches, and residual stress leading to undesirable lifetime variations (Kim et al., 2013).

The empirical models such as the Paris-Erdogan law generally have limited applicability to thermoplastics given the complex characteristics of SCG and associated PZ (Almomani & Mourad, 2023; Chudnovsky, 2014; Lang et al., 1997; Maiti & Mourad, 1995a, 1995b). Such SCG behavior can't be simulated using the conventional empirical equations and based on phenomenological grounds. The lifetime discrepancy of HDPE butt-fusion joints and parent material has been investigated in the past. Mikula et al. (Mikula et al., 2015; Mikula et al., 2017), utilized the conventional Paris-Erdogan law to study the effect of weld bead on PE lifetime induced by circumferential cracks. Li et al. (Li et al., 2016), relied on extrapolation to predict this lifetime variation using CRB specimens. Kalyanam et al. (Kalyanam et al., 2015), used empirical equations to investigate the impact of standards dimension ratio (SDR) on the SCG failure time using circumferentially cracked HDPE pipes. Pfeil et al. (Pfeil et al., 1993), developed an empirical crack growth model based on the creep compliance to predict the life expectancy of PE pressurized pipes joints. The fracture model, however, relies on the time–temperature superposition shift and power law correlation, and fails to simulate the discontinuous SCG patterns, jump lengths, and respective periods. Popelar et al. (Popelar et al., 1991), earlier, using the same crack growth model demonstrated that SCG lifetime of a butt joint is significantly lower than that of a pipe. The same detrimental effect of the joint beads on the failure time was reported by Bergström et al. (Bergström et al., 2004). Lai et al. (Lai et al., 2022), used an empirical expression to investigate the variation of creep life of HDPE pipe joints. The developed correlation is further constraint to a single temperature and stress level.

The crack layer (CL) theory proposed by A. Chudnovsky (Chudnovsky, 1984), which was recently expanded by Wee et al. (Wee et al., 2023) to model overload induced SCG retardation, offers an effective framework that can reproduce such complex continuous and discontinuous SCG modes and their transition. In the CL theory, the crack and the PZ are treated as a coupled system. This way, the physical interaction amongst the two can be captured. Using thermodynamics of irreversible processes (TIP), the thermodynamic forces (TFs) responsible for the crack and PZ growth can be determined which accounts for the energy dissipation needed for the generation of micro-damages (Chudnovsky & Moet, 1985; Sehanobish et al., 1986; Wee & Choi, 2016). Consequently, the continuous and discontinuous SCG kinetics of HDPE can be reproduced using the CL theory and even the transition between the two (Byoung-Ho Choi et al., 2009; B. H. Choi et al., 2009; Zhang et al., 2014). The CL simulation not only provides the HDPE component lifetime or SCG rate, but also produce the complete crack and PZ damage growth process. This gives the theory another advantage for industrial settings over the conventional empirical models.

Despite the various applications present for the CL theory (Almomani et al., 2024; Wee et al., 2021; Wee & Choi, 2020; Wee, Chudnovsky, et al., 2020), its deployment to complex and large-scale critical geometries is still lacking. The existing CL model for pipes can only be applied to longitudinally oriented cracks that are initiated from a pipe's inner or external surface (Wee, Park, et al., 2020). The majority of the pressurized HDPE pipes suffer from poor joining and such butt-joints likely end-up as crack initiating sites. A SCG model based on the CL theory for HDPE pipes circumferential and butt-fusion joints induced cracks is hence needed for their lifetime predictions. Therefore, the objective of this work is fourfold: (i) to develop a CL model for pipes with circumferential internal and external cracks for multiple standard dimension ratios, i.e., $6 \leq \text{SDR} \leq 22$, (ii) to extend the proposed model to butt-fusion edge and center-line induced pipe cracks, (iii) to investigate the influence of SDR, internal pressure, and temperature on the lifetime

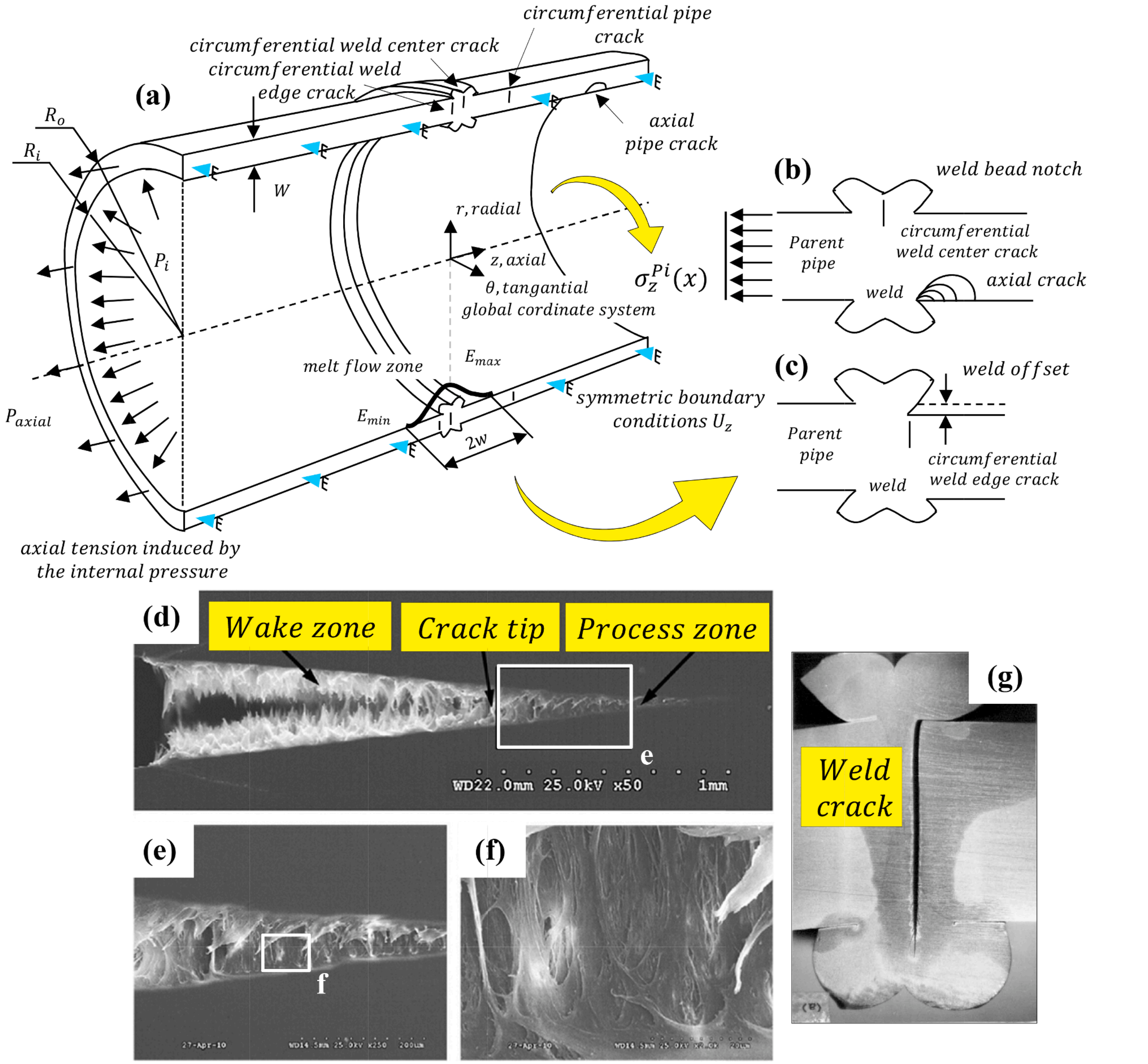

Fig. 1. (a) A HDPE welded pipe with a butt-fusion joint containing weld center, weld edge and pipe circumferential cracks. (b) A butt-joint center crack induced by the presence of the bead with axial stress distribution $\sigma_z^{Pi}(x)$ in the wall induced by the internal pressure P_i. (c) A weld center crack triggered by the removal of the weld bead. (d) HDPE scanning electron microscopy (SEM) images of the CL process zone at 50x, (e) the active zone with broken and intact fibers at 250x, and (f) drawn fibers inside the active zone at 2000x at 23 °C (Chudnovsky et al., 2012). (g) A butt-fusion joint induced SCG initiated from the bead edge (Parmar, 1986).

variation of internally and externally cracked HDPE pipes, and (iv) to compare the proposed model simulations with experimental discontinuous SCG results from pipes. Overall, this study aims to expand the applicability of the CL model for a reliable application to butt-fusion welded HDPE pipes integrity and remaining life assessments.

2. Methodology

An overview of the procedure used to develop and implement the CL model of butt-fusion joints induced SCG in HDPE pipes is illustrated. Fig. 2 displays the CL modeling implementation flowchart which consists primarily of three main modules. The first module necessitates the provision of the essential Fracture Mechanics parameters for the numerical module such as the energy release rate (ERR), stress intensity factor (SIF), and crack opening displacement (COD) solutions. The second module is the material properties module that explores experimental data evaluating a set of parameters such as the specific energy of transformation γ^{tr}, the natural drawing ratio λ, the crack kinetic coefficient k_{CR}, the fracture toughness K_{Ic}, and the plane-strain elastic modulus E'. The third module is the numerical module which takes the input of the material properties and fracture mechanics modules providing solutions to the CL constitutive equations. It also includes displaying the results of the CL simulations.

Estimation of the SIF and COD can be done using approximate analytical expressions in order to compute the crack and PZ thermodynamic forces. Employing the Green's function, instead, can be simpler alternative which is adopted in this work explained in section 3.3. The SIF and COD can then be obtained by integrating the Green's functions over the length where the load is applied. Since HDPE pipe applications can be highly critical, it would be essential to develop specific GFs for the exact crack geometry, such as the butt-fusion joint shape. For that, using the concept of "substitute geometry" existing GFs for simple geometries is used which will be explained in section 3.4.

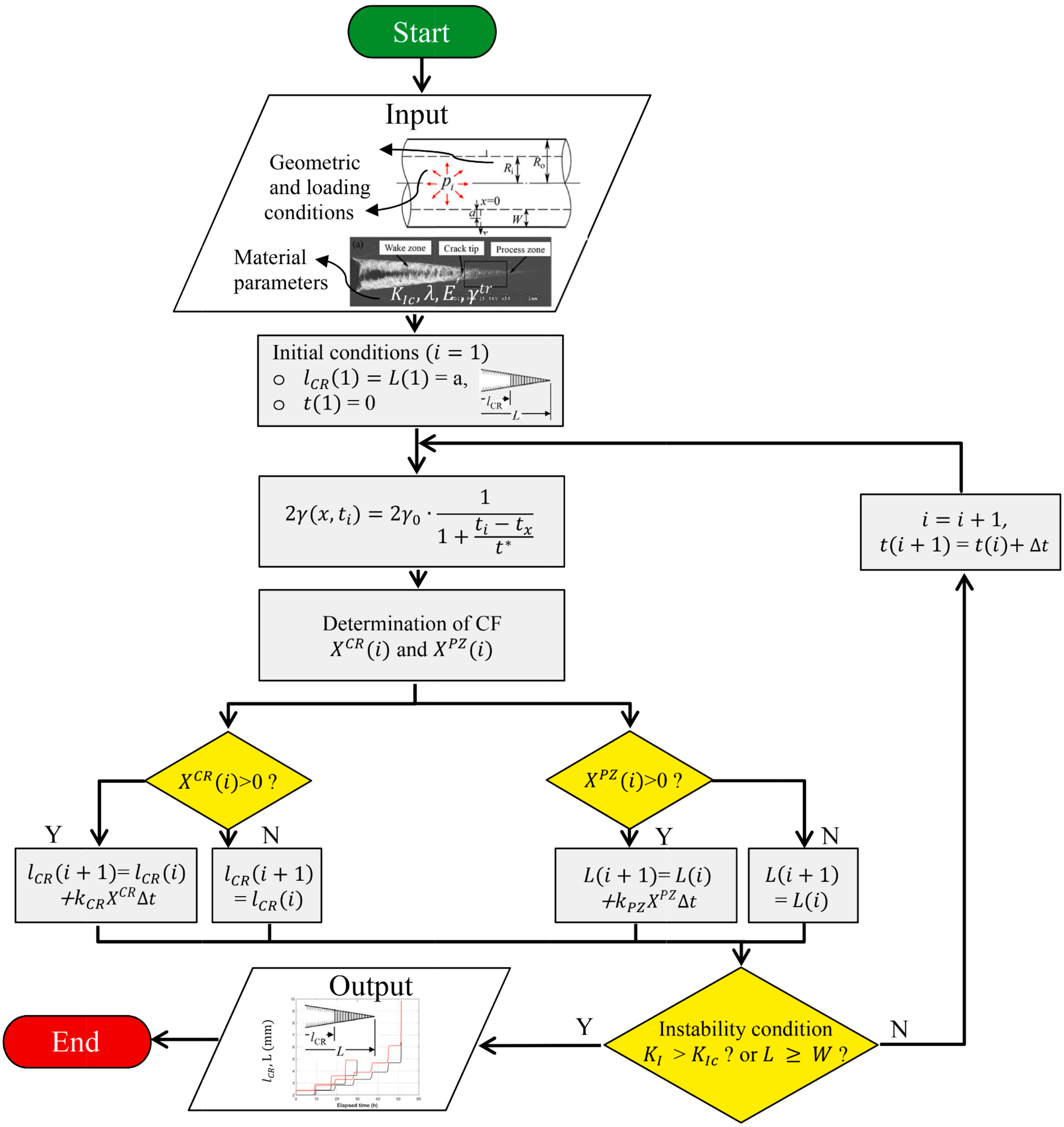

Fig. 2. Crack layer (CL) growth algorithm flowchart for the crack and crack layer, denoted l_{CR} and L, starting from the input geometry, loading and material parameters till the instability criterion. This includes the determination of the thermodynamic forces for the crack and PZ, separately.

Based on the description of CL theory for HDPE, a numerical simulation is programmed using the commercial software MATLAB, and the algorithm of the program is shown in Fig. 2. The algorithm of the CL system simulation is primarily made based on a loop statement, along with multiple stages that dictate a single loop of calculation. Input parameters including the geometric conditions, loading conditions, and material parameters were used to determine the TFs for CL growth. In this study, two termination conditions were applied: (1) an SIF at the crack tip that was larger than the fracture toughness K_{Ic} of the HDPE, and (2) a large displacement owing to the absence of an elastic ligament i.e., $L \geq W$. If one of the instability conditions is satisfied, then the simulation is terminated. The final output comprises the kinetics of crack and PZ growth with time, including the final lifetime.

3. Development of CL model

3.1. Application of the CL theory to high density polyethylene

The application of the CL theory to modeling SCG of HDPE is facilitated by several key characteristic features. The crack tip in PE is typically coupled and surrounded with a PZ. With the crack at the center, this PZ appears as a narrow wedge strip, as shown at low magnification in Fig. 1d. Its morphology of the drawn fibers undergoes a gradual change in dimension from coarse to fine membranes toward the crack tip, as displayed in white in Fig. 1e. Depending on the temperature and the stress level applied, the fracture surface would show stepwise striations that indicate the discontinuous SCG mode. Ahead of the crack tip lies an active zone (AZ) with intact fibers that is part of the PZ and

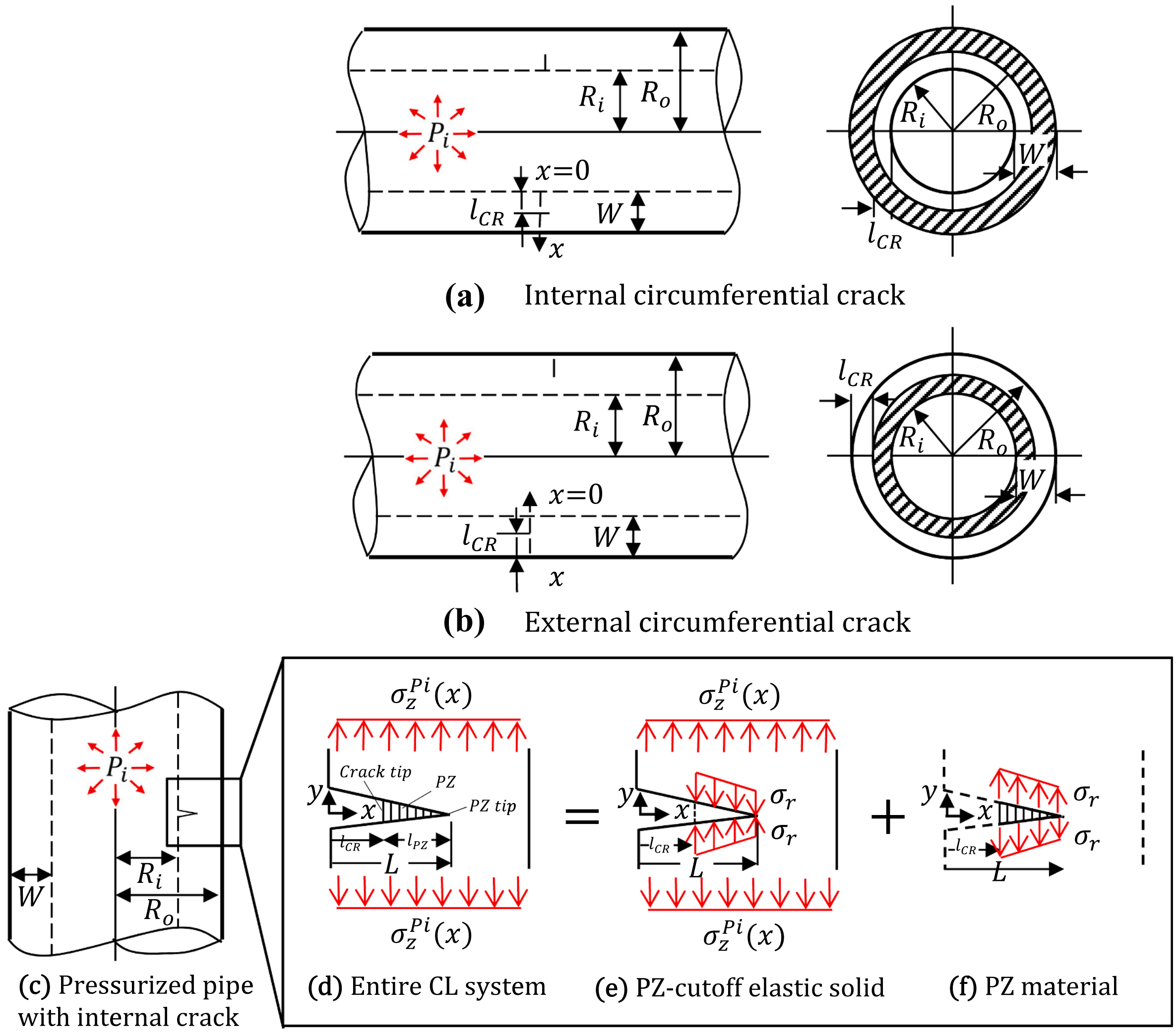

Fig. 3. Pipe geometry cross and side views with (a) an internal and (b) an external circumferential crack. The pipe has a crack length l_{CR}, along the wall W, with an inner and outer diameter denoted R_i and R_o. Superposition methodology for the CL system of (c) the pipe subject to an axial stress σ_z^{Pi} induced by the internal pressure P_i with an initial internal circumferential crack. (d) entire CL system including the crack l_{CR} and the PZ l_{PZ}; (e) PZ-cutoff elastic solid with drawing stress σ_r at the PZ boundary; (f) PZ material. This superposition principle, through its additive property, allows for the summation of the generated SIF and COD.

primarily carry extreme load and undergo creep. The fracture of those intact membranes in the AZ translates into the crack advancement in material space. The remnant part of the PZ with ruptured fibers left behind is called the wake zone (WZ). The CL in HDPE can grow in either a continuous or discontinuous mode or a mixed manner, depending on the temperature and the stress intensity factor (SIF). For instance, the CL may start as continuous SCG then as the crack length l_{CR} increases it shifts into discontinuous propagation.

The original bulk material is separated from the drawn fibers by a sharp boundary owing to HDPE simple PZ geometry. The elastic interaction between the matrix and the AZ is considered through the closing stress along the boundary of the drawn and original PE material. A unique dendroid texture with oriented fibers results from such interaction as shown in the boxed area of Fig. 1f in Fig. 1d and 1e. Critical insights on the crack growth mechanisms and kinetics are revealed from such observations on the SCG fracture process. Consequently, in HDPE, the crack-PZ interaction should always be considered in a crack growth model and inherent driving forces. The thermodynamic forces (TFs) behind the CL evolution are derived from the system Gibbs free energy (G). The derivation of those forces for a plain pipe and butt-joint induced circumferential crack will be discussed next.

3.2. Thermodynamic forces for CL growth

A pipe with an initial circumferential crack at either the internal or external surface subject to arbitrary axisymmetric loading condition including internal pressure P_i is considered, as illustrated in Fig. 3a and 3b. The pipe has a crack length l_{CR}, an inner radius R_i, an outer radius R_o, and a wall thickness W. The CL length denoted by L, is composed of the sum of l_{CR}, and the wedge-shaped PZ length, l_{PZ}. In the CL theory, the undamaged elastic solid, the crack and the PZ are considered as separate phases. The principle of superposition is followed which uses the additive property of the SIF and is illustrated in Fig. 3c over a schematic of a pipe. The thermodynamic forces (TFs) for each phase growth are then derived from the variation in the system Gibbs free energy (∂G) with regard to the migration of each phase boundary. Hence, there would be two CL thermodynamic forces (TFs), one for the crack and another for the PZ growth, i.e., X^{CR} and X^{PZ}. The general expressions for the crack and PZ driving forces are formulated as (Zhang et al., 2014):

$$X^{CR} = -\frac{\partial G}{\partial l_{CR}} = J_I^{CR} - 2\gamma; \tag{1}$$

$$X^{PZ} = -\frac{\partial G}{\partial l_{PZ}} = J_I^{PZ} - \gamma^{tr} R_I = \frac{K_{tot}^2}{E'} - \gamma^{tr}\frac{\delta_{tot}}{\lambda - 1} \tag{2}$$

Table 1
$\beta_i(a/W)$Values for a pipe internal circumferential crack ($\beta_1 = 2.0$) (Wu & Xu, 2022).

a/W	R_o/R_i(SDR)					
	1.1 (22)		1.25 (10)		1.5 (6)	
	β_2	β_3	β_2	β_3	β_2	β_3
0.001	1.342602	0.219149	1.341622	0.219067	1.340808	0.218999
0.01	1.345618	0.218874	1.335696	0.218077	1.327118	0.217461
0.1	1.590968	0.210598	1.460387	0.206227	1.337426	0.199923
0.2	2.182937	0.279093	1.838987	0.240906	1.543050	0.201373
0.3	2.966087	0.518024	2.359112	0.353070	1.880252	0.228260
0.4	3.876025	0.956021	2.975577	0.556391	2.320738	0.293442
0.5	4.887797	1.613671	3.688123	0.836812	2.879403	0.373318
0.6	5.969588	2.542888	4.597550	1.086138	3.720394	0.282110

Table 2
$\beta_i(a/W)$Values for a pipe external circumferential crack ($\beta_1 = 2.0$) (Wu & Xu, 2022).

a/W	R_o/R_i(SDR)					
	1.1 (22)		1.25 (10)		1.5 (6)	
	β_2	β_3	β_2	β_3	β_2	β_3
0.001	1.345356	0.219039	1.344383	0.219303	1.344005	0.219269
0.01	1.363552	0.220440	1.361639	0.220588	1.358950	0.220178
0.1	1.693586	0.211179	1.658827	0.221305	1.642026	0.236039
0.2	2.374577	0.310423	2.220391	0.302955	2.126612	0.307427
0.3	3.235805	0.629616	2.903491	0.535156	2.727109	0.447166
0.4	4.252173	1.135648	3.700904	0.856735	3.430452	0.667894
0.5	5.334308	1.971685	4.603010	1.310880	4.270887	0.951407
0.6	6.606864	2.902259	5.671079	1.850749	5.406120	1.182968

where J_I^{CR} is the energy release rate (ERR) due to one step crack growth into the PZ. Likewise, J_I^{PZ} is the ERR due to PZ unit advancement. Meanwhile, γ and γ^{tr} are the specific fracture energy (SFE) of the PZ and the HDPE transformation energy for a single unit volume into drawn state. R_I is the volumetric change in the PZ medium with respect to the growth of L. In addition, K_{tot} is the sum of the SIFs determined by superposition, i.e., the linear summation of the P_i driven axial stress σ_z^{Pi} and σ_{dr}. For HDPE, a clear boundary between the undamaged material and the PZ is observed, wherein σ_{dr} is considered the boundary traction. Furthermore, if the ligaments within the PZ are assumed to be drawn by their natural drawing ratio λ, R_I can be written as $R_I = (\lambda - 1)^{-1}\delta_{tot}$. Herein, δ_{tot} is the crack opening displacement (COD) at the PZ-cutoff elastic solid crack tip, shown in Fig. 3e. The non-zero value of the K_{tot} is what makes the difference between the CL and Dugdale-Barenblatt (DB) model equilibrium PZ which requires $K_{tot} = 0$.

The CL system thermodynamic forces for a thin PZ, comprising of transformed and drawn material, were derived for HDPE in (Stojimirovic et al., 1992; Zhang et al., 2014). The expression ($J_I - 2\gamma$) in Eq.(1) and Eq.(2), following the conventional terminology, is the thermodynamic force conjugate to the crack growth rate $\dot{l}_{CR}$. In other words, it is the crack driving force. Crack equilibrium condition would hence correspond to vanishing this force. When the TFs are zero, i.e., $X^{CR} = 0$ and $X^{PZ} = 0$, an equilibrium configuration of the CL is reached. A thermodynamic system has the tendency to go back to a stationary state, at small deviations from equilibrium. However, fibers creep within the PZ is an irreversible process. Thus, there is no return whenever the crack advances into the PZ through fibril breakdown. Once the TFs for the crack and PZ are developed, the rate of crack l_{CR} and crack layer L lengths are formulated by a linear relationship, as follows (Zhang et al., 2014):

$$\underline{i} = \mathbf{k}\underline{X}, \tag{3}$$

where $\underline{i}$ is a vector comprised of the crack l_{CR} and crack layer L; $\underline{X}$ is the X^{CR} and X^{PZ} vectors; $\mathbf{k}$ is a kinetic coefficient tensor of 2 x 2 size. According to Onsager's reciprocal theorem, the kinetic coefficient tensor k_{ij} has symmetry, and thus, $k_{ij} = k_{ji}$. The tensor $\mathbf{k}$ includes constant indices, owing to quasi-static evolution of the CL during the SCG process. Additionally, it can be simplified to a diagonal matrix, neglecting any cross effects. A small incremental crack and PZ lengths can be calculated, if Eq. (3) is multiplied by a small-time increment Δt. With that, by applying a time-marching loop to Eqs. (1)-(3), the CL growth complete simulation can be achieved. To obtain K_{tot} and δ_{tot}, the Green's function for the internal and external circumferential pipe crack are developed, respectively, in the next section.

3.3. Green's function for internal and external circumferential cracks in pipe geometry

3.3.1. SIF Green's function

The Green's function for a SIF, G^{SIF}, results from a unit dipole force on the crack face, i.e., a single upward and downward unit force applied at a specific location along the crack x. The x-coordinate for the internal and external cracks, is measured from the respective outer and inner surface. Therefore, the G^{SIF} would be a function of the inner and outer radii of the pipe, R_i and R_o, respectively; the crack length a, and the unit force position x. The methodology described herein will be applied to construct the SIF Green's function for a pipe with circumferential cracks. The SIF Green's function for an internal or external crack acting on an arbitrary point along the crack line can consequently be expressed as follows from Wu et al. (Wu & Xu, 2022):

$$G_{int,ext}^{SIF}(a, x, W) = \frac{1}{\sqrt{2\pi a}} \cdot \sum_{i=1}^{3} \beta_i(\alpha) \cdot (1 - \xi/\alpha)^{i-3/2} \tag{4}$$

$$\begin{cases} \beta_1(\alpha) = 2 \\ \beta_2(\alpha) = \left\{ \alpha \overset{\text{Å}}{F_1}(\alpha) + [3F_2(\alpha) + F_1(\alpha)]/2 \right\} / f_r(\alpha) \\ \beta_3(\alpha) = \left\{ \alpha \overset{\text{Å}}{F_2}(\alpha) - F_1(\alpha)/2 \right\} / f_r(\alpha) \end{cases}$$

where the coefficient β_i is a function of the geometry of the entire cracked solid including the crack length a. Meanwhile, $\alpha = a/W$ and $\xi = x/W$. The reference load case used to construct the G^{SIF} is a uniform

Table 3
μ_i Values of the fitted $f_i(a/W)$ functions for an internal crack using seventh order polynomials.

R_o/R_i(SDR)	$f_i(\alpha)$	μ_0	μ_1	μ_2	μ_3	μ_4	μ_5	μ_6	μ_7
1.1 (22)	f_2	1.343	−1.767	23.082	−78.474	228.741	−402.545	348.975	−90.946
	f_3	0.2191	−0.1445	−2.743	35.789	−166.879	397.583	−431.470	151.782
1.25 (10)	f_2	1.343	−0.958	28.067	−84.707	206.386	−322.376	262.987	−68.842
	f_3	0.219	−0.076	−3.488	41.438	−146.181	305.277	−316.854	114.576
1.5 (6)	f_2	1.342	−1.766	20.085	−76.472	228.750	−398.530	339.981	−89.930
	f_3	0.2180	−0.1433	−2.721	34.770	−166.880	396.591	−431.443	152.797

Table 4
μ_i Values of the fitted $f_i(a/W)$ functions for an external crack using sixth and seventh order polynomials.

R_o/R_i(SDR)	$f_i(\alpha)$	μ_0	μ_1	μ_2	μ_3	μ_4	μ_5	μ_6	μ_7
1.1 (22)	f_2	1.343	1.433	21.495	−78.680	239.613	−442.844	428.174	−147.693
	f_3	0.2191	0.124	−2.504	45.218	−199.319	481.218	−567.015	246.155
1.25 (10)	f_2	1.346	0.956	29.903	−101.195	238.188	−300.878	158.004	–
	f_3	0.216	1.084	−25.351	202.552	−616.095	883.881	−482.779	–
1.5 (6)	f_2	1.350	1.441	21.481	−78.662	239.622	−442.844	428.187	−147.684
	f_3	0.2188	0.131	−2.511	46.227	−198.325	482.240	−568.031	247.167

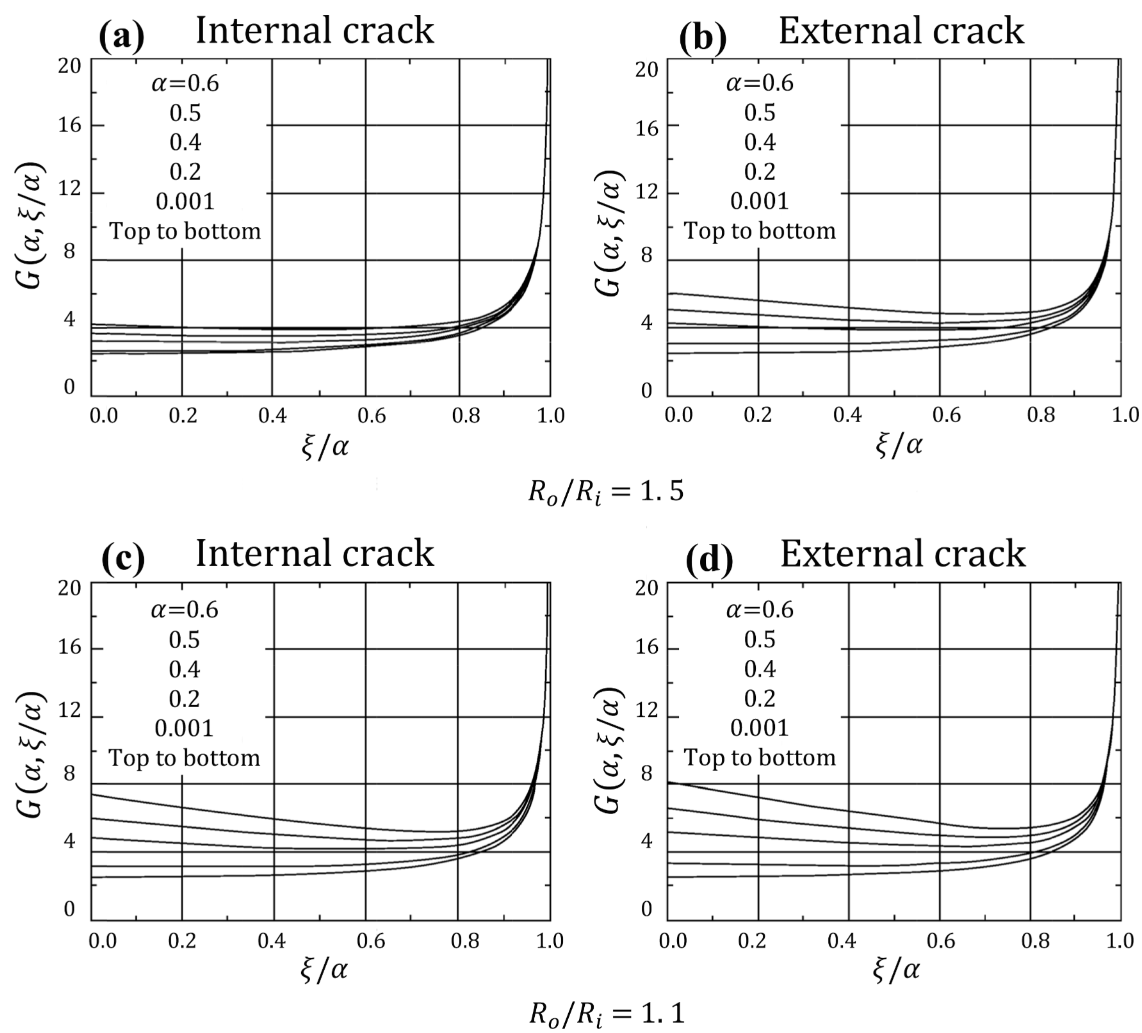

Fig. 4. Comparison of various Green's functions (GFs) for pipe with internal and external circumferential cracks at several a/W ratios for (a and b) $R_o/R_i = 1.5$ and (c and d) $R_o/R_i = 1.1$. Herein the crack-to-width ratio a/W is denoted α, whereby ξ is unit load location to width ratio x/W (Wu & Xu, 2022). (For interpretation of the references to color in this figure legend, the reader is referred to the web version of this article.)

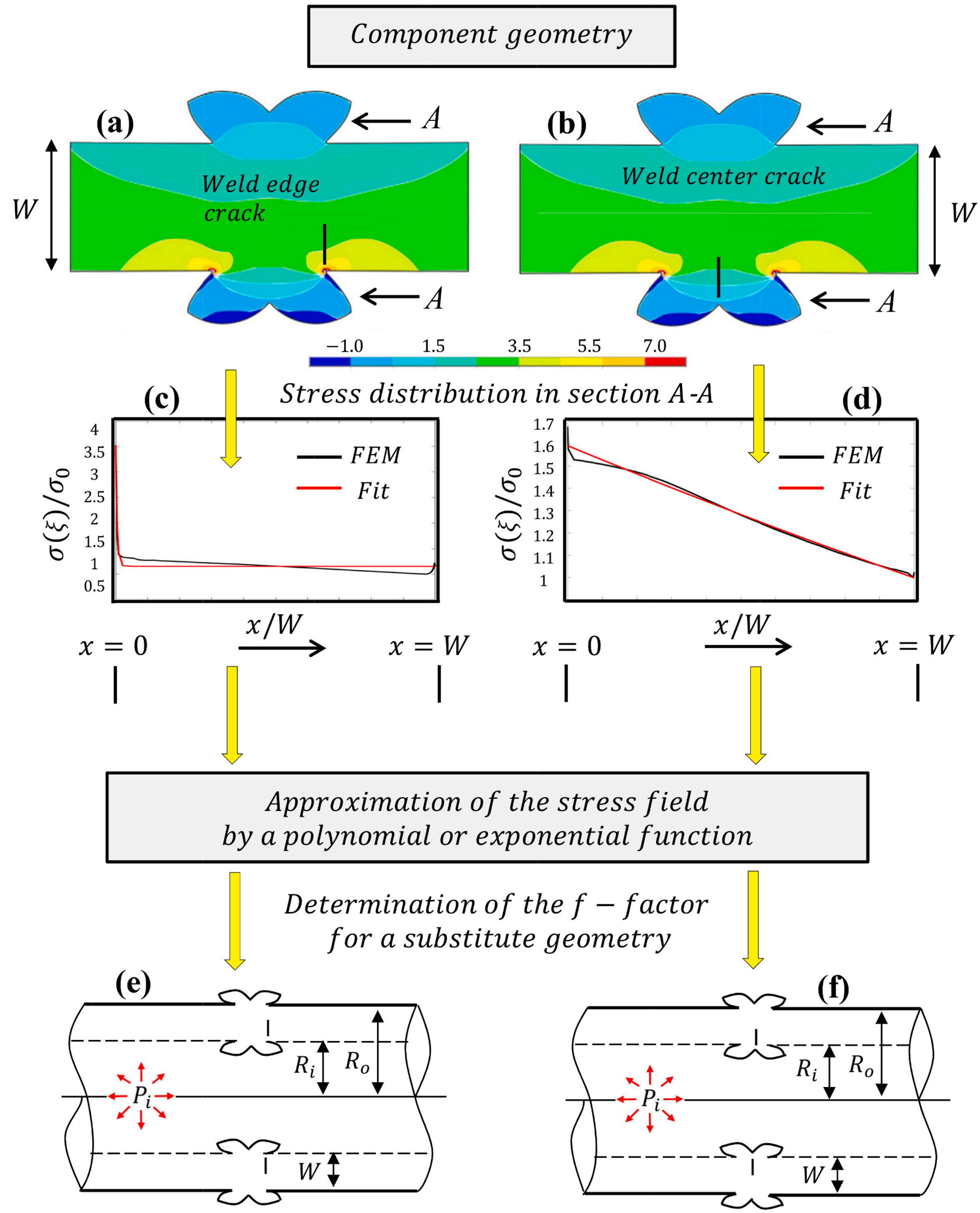

Fig. 5. Determination of the SIFs for the circumferential crack for a complex geometry, e.g., cracked butt-fusion joint in a HDPE pipe, by using substitute geometries. The process starts with the determination of the uncracked geometry stress distribution $\sigma(\xi)$ by FEM, followed by an approximation of the field by a polynomial or exponential function. The resultant normalized stress line $\sigma(\xi)/\sigma_0$ is then used for the determination of the weld Green's functions, G_{WE}^{SIF} and G_{WC}^{SIF}. (For interpretation of the references to color in this figure legend, the reader is referred to the web version of this paper.). (For interpretation of the references to color in this figure legend, the reader is referred to the web version of this article.)

crack line stress with $\sigma(\xi)/\sigma_0 = 1$. Where $F_i(\alpha)$ is of the following form (Wu & Xu, 2022):

$$\begin{cases} F_1(\alpha) = 4f_r(\alpha) \\ F_2(\alpha) = \dfrac{5}{2}\left[\sqrt{2}\,\pi\phi(\alpha) - \dfrac{8}{3}f_r(\alpha)\right] \end{cases} \tag{5}$$

where $f_r(\alpha)$ and $\phi(\alpha)$ are of the following forms (Wu & Xu, 2022):

$$f_r(\alpha) = \sum_{n=0}^{N} \lambda_n \alpha^n \tag{6}$$

Table 5
A, λ and B values of the fitted $f(x/W)$ functions for the stress line using an exponential fit.

$f_i(x/W)$	Weld edge			Weld center		
	A	λ	B	A	λ	B
f_{WE}, f_{WC}	2.375	−235.488	1.152	3.710	−0.174	− 2.118

$$\phi(\alpha) = \alpha^{-2}\int_0^\alpha s f_r^{\,2}(s)ds = \sum_{i=0}^{N}\sum_{j=0}^{N}\lambda_i\lambda_j\frac{\alpha^{i+j}}{i+J+2} \tag{7}$$

where λ_n, λ_i and, λ_j are fitting coefficients. The numerical $\beta_i(\alpha)$-data for a circumferential crack in a pipe from Wu et al. (Wu & Xu, 2022) are given in Table 1 for an internal crack and Table 2 for an external crack. The data correspond to discrete α-values of $0 \le \alpha \le 0.6$. To facilitate the application, the $\beta_i(\alpha)$-data coefficients were fitted by polynomial equations with the variable crack length a as follows:

$$f\left(\frac{a}{W}\right) = \sum_{i=0}^{k}\left[\mu_i\left(\frac{a}{W}\right)^i\right] \tag{8}$$

In this study, the $f_i(a/W)$ functions were fitted using sixth and seventh order polynomials ($k = 6$ and 7), as displayed in Table 3 for an internal crack and Table 4 for an external crack. In addition, $f_i(a/W)$ was

Table 6
Elastic Modulus $E_i(x)$ values within the butt-joint zones and for the parent material (Veselý et al., 2009).

$E_i(x)$	Unit	Elastic Modulus		
		Parentmaterial(P)	*Weldedge(WE)*	*Weldcenter(WC)*
E_P, E_{WE}, E_{WC}	MPa	1000	1040	1070

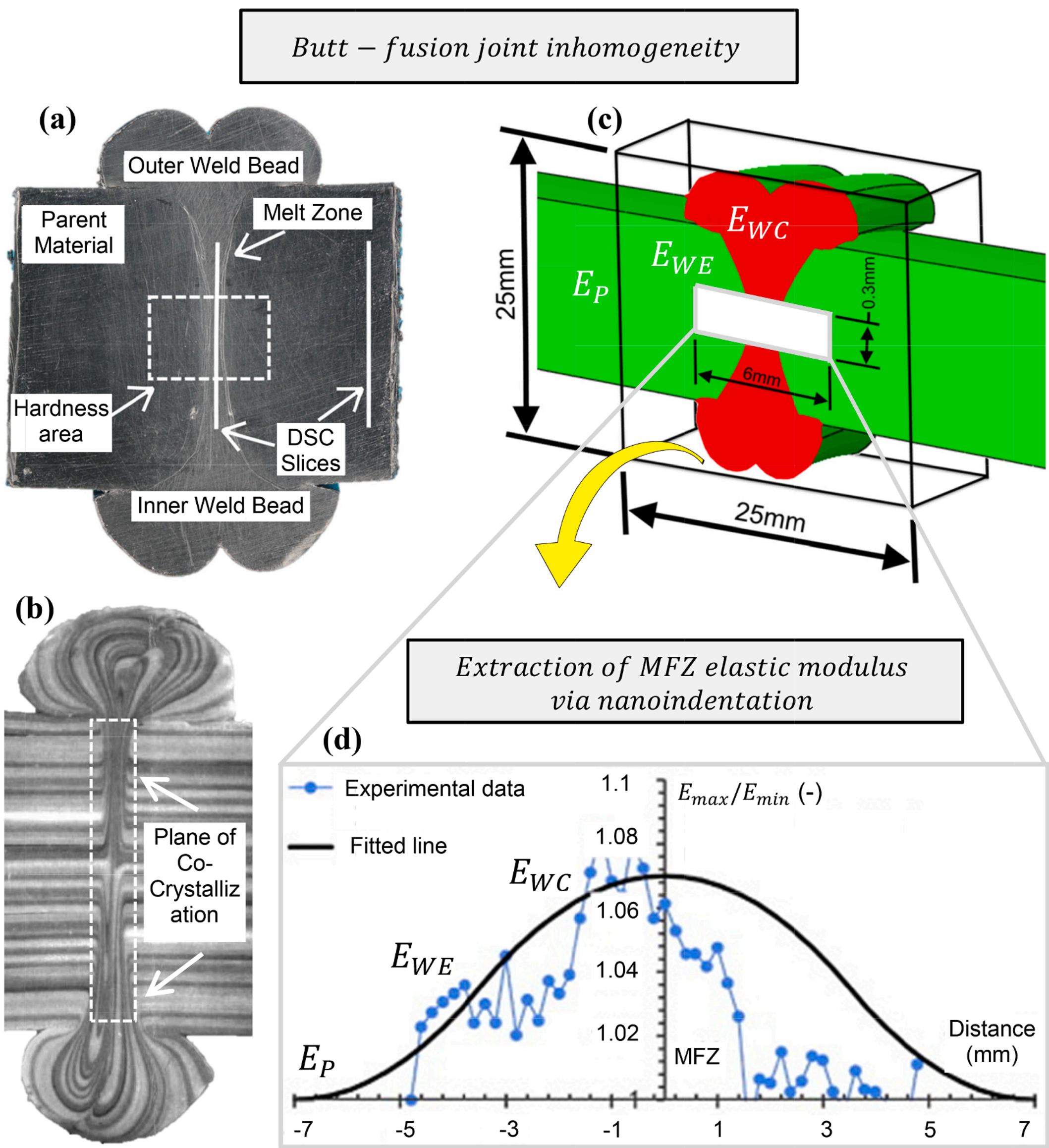

Fig. 6. Incorporation of material inhomogeneity within the butt-fusion joint for the CL model material properties. (a) Macrograph of a typical butt-joint with the visible weld features labelled, including the melt flow zone (MFZ) (Shaheer et al., 2017). (b) Micrograph of the butt-joint revealing the bead structure, flow orientation, the radial melt flow, and the plane of co-crystallization ("TN-51 – Polyethylene Pipe Butt Fusion Structure, Process, and Terminology," 2018). (c) Sketch of welded HDPE pipe section showing the location of the weld, with the MFZ and the weld beads in red highlighting the nanoindentation 6 × 0.3 mm grid. (d) Normalized Young's modulus from PE micro indentation tests (Veselý et al., 2009), outlining the WE elastic modulus E_{WE}, WC elastic modulus E_{WC}, and parent material elastic modulus E_P. (For interpretation of the references to color in this figure legend, the reader is referred to the web version of this paper.). (For interpretation of the references to color in this figure legend, the reader is referred to the web version of this article.)

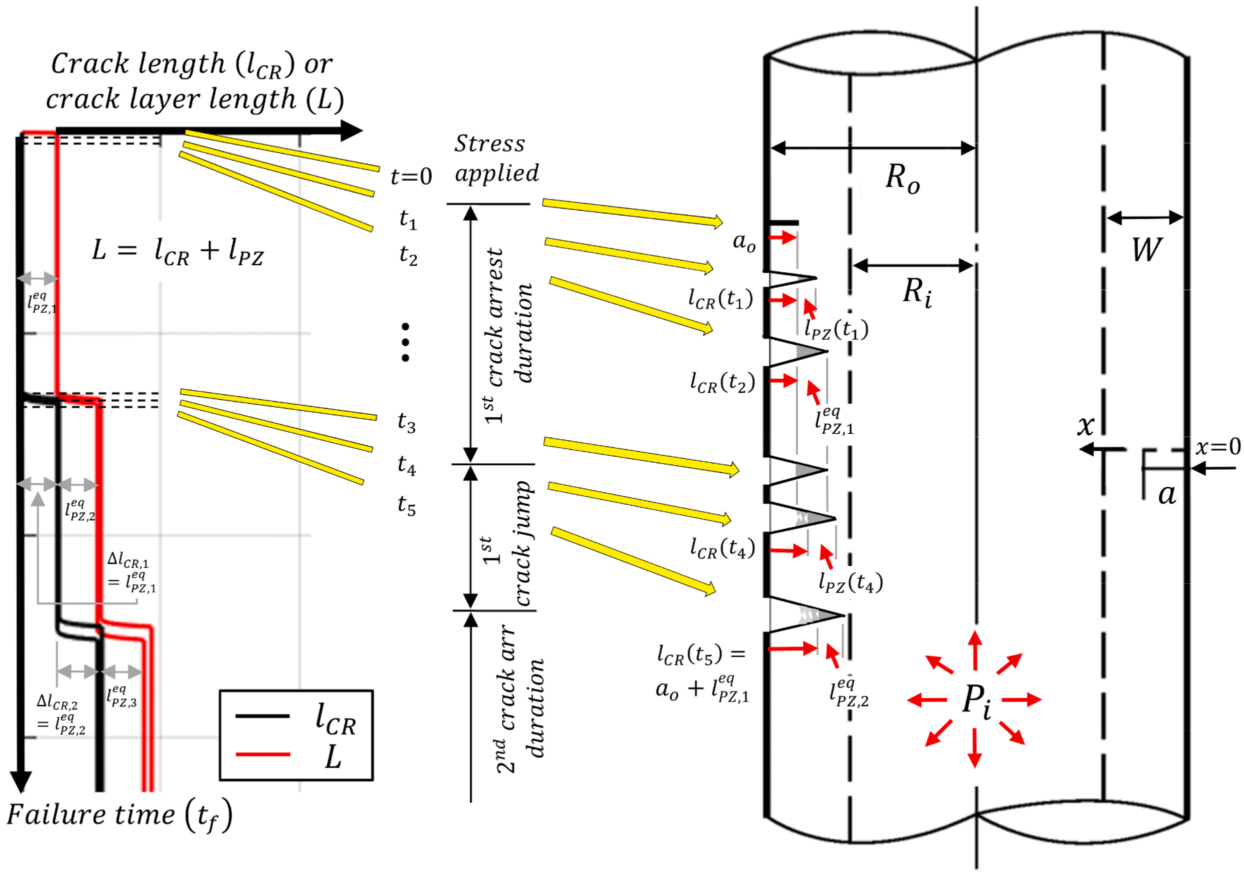

Fig. 7. The CL discontinuous SCG mechanism descriptive schematic of an HDPE pipe with an external circumferential crack under internal pressure P_i induced axial stress $P_iR_i/2W$ loading, where l_{CR} and L are the crack and crack layer length. The schematic illustrates the 1st and 2nd crack arrest, jump and durations starting at t_i = 0 at the onset stress application.

fitted to three R_o/R_i ratios corresponding to SDR 22, 10 and 6, i.e., thin pipes to thicker ones. Fig. 4 shows representative GF curves for internal and external circumferential cracks with for $R_o/R_i = 1.5$ and 1.1 at several a/W ratios. The crack-to-width ratio a/W is denoted α, meanwhile ξ is the unit load location to the width ratio x/W. The WF using the fitted β_i expressions are in good agreement with that by direct computations with less than 0.5 % differences. This demonstrates the sufficient accuracy of the proposed SIF Green's function, for all the crack-to-width ratio a/W cases. With that, one can evaluate the resulting SIF owing to any axial stress distribution by integrating the SIF GF over the cracked face.

In the driving force evaluation, only the stress normal to the crack plane is explicitly considered. In other words, for either the internal or external circumferential crack in the pipe, the stress in the axial direction σ_z^{Pi} is considered in the SIF calculation, while the stress in the hoop direction σ_θ^{Pi} is neglected. This is rather a simplification, since the hoop stress σ_θ^{Pi} would only slightly increase the crack driving force combined with axial tension (Huang et al., 2020; Kim et al., 2002; Xu et al., 2010), under biaxial loading, or the COD through local crack bulging (Jayadevan et al., 2004; Rahman et al., 1998). With that, the resultant axial stress σ_z^{Pi} SIF can be calculated by integrating the GF, G^{SIF}, over the crack face. For a pipe geometry, the SIF due to internal and external pressures, P_i and P_o, for an internal circumferential crack, is expressed as follows:

$$K_{int}^{Pi} = \int_0^L \frac{P_iR_i^2 - P_oR_o^2}{R_o^2 - R_i^2} \bullet G_{int}^{SIF}(L, R_o, R_i; x)dx \tag{9}$$

where L is the CL length, P_o is the outer pressure and set to zero, and x is measured from the pipe inner wall. Meanwhile, the SIF for an external circumferential crack is expressed as follows:

$$K_{ext}^{Pi} = \int_0^L \frac{P_iR_i^2 - P_oR_o^2}{R_o^2 - R_i^2} \bullet G_{ext}^{SIF}(L, R_o, R_i; x)dx \tag{10}$$

where x is measured from the pipe outer wall. The above expressions are used to estimate the ERR due to a unit crack advancement J_1^{CR}. Whereas the PZ boundary traction are assumed constant through the material drawing stress (σ_{dr}). Thus, the SIF due to σ_{dr} is obtained by numerically integrating the pipe inner crack GF, G_{int}^{SIF}, as follows:

$$K_{int}^{dr} = -\sigma_{dr} \int_{l_{CR}}^L G_{int}^{SIF}(L, R_o, R_i; x)dx \tag{11}$$

Meanwhile, for an external circumferential crack, the pipe external crack GF, G_{int}^{SIF}, is integrated instead, as follows:

$$K_{ext}^{dr} = -\sigma_{dr} \int_{l_{CR}}^L G_{ext}^{SIF}(L, R_o, R_i; x)dx \tag{12}$$

K_{int}^{dr} and K_{ext}^{dr} are then used to estimate the ERR due to PZ unit advancement J_1^{PZ}. The total SIF K_{tot} is eventually calculated from the superposition of the SIF resulting from P_i and σ_{dr}, i.e., $K_{tot} = K_{Pi} + K_{dr}$. The determination of the COD Green's functions is discussed next.

3.3.2. COD Green's function

The COD Green's function can be used to the pipe crack l_{CR} and crack layer L displacement. The ERR calculated in the previous section outlines the strain energy physical change due to the crack propagation. Using Castigliano theory, the total displacement δ_{tot} can otherwise be determined directly (Kadota & Chudnovsky, 1992). The COD for an internal or an external circumferential crack in a pipe geometry can accordingly be calculated. By double integrating the SIF Green's

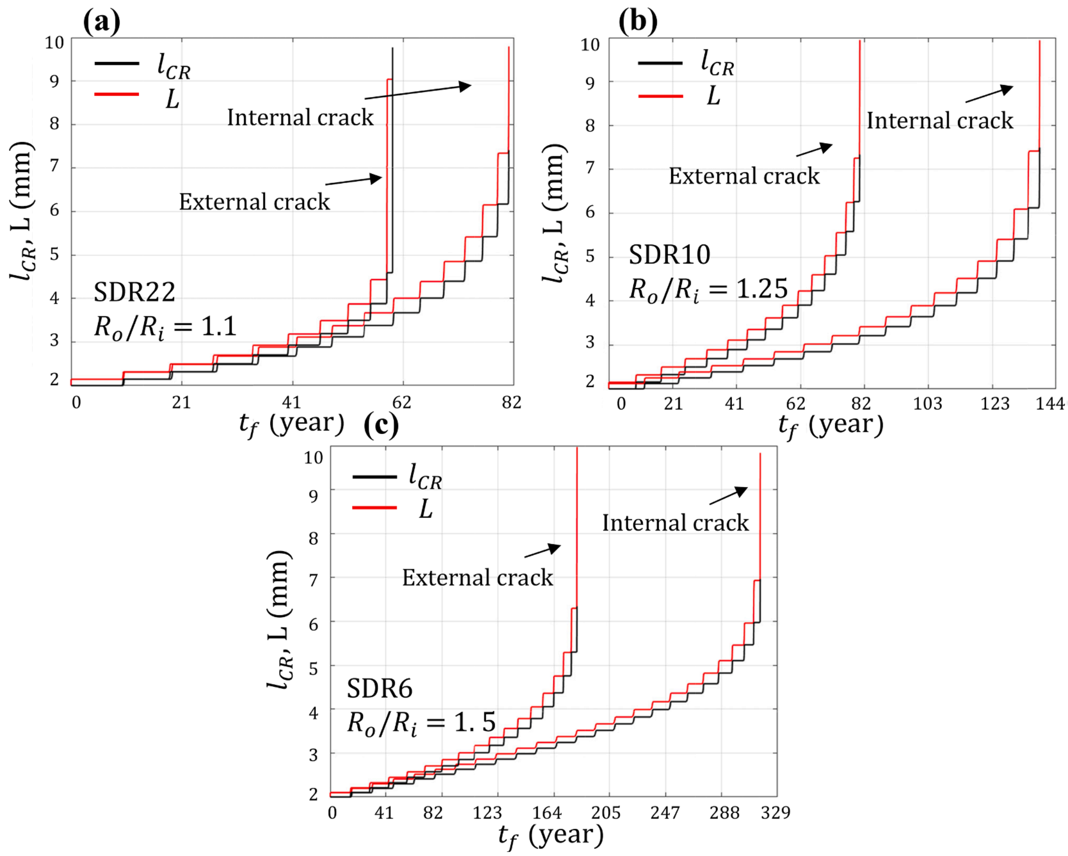

Fig. 8. The crack and CL system growth simulation versus the elapsed time of a pressurized pipe under nominal axial stress $P_iR_i/2W = 4.5$ MPa, for (a) SDR22; (b) SDR10; (c) SDR6. (For interpretation of the references to color in this figure legend, the reader is referred to the web version of this paper.).

function over the crack face, the COD profile at the crack tip ($x_1 = l_{CR}$) can be evaluated for internal pressure P_i induced axial stress σ_z^{Pi} as follows:

$$\delta_{int,ext}^{Pi} = \frac{2\sigma_z^{Pi}}{E'} \int_x^{l_{CR}} \int_0^{\xi} G_{int,ext}^{SIF}(\xi, R_o, R_i, x_0) \cdot G_{int,ext}^{SIF}(\xi, R_o, R_i, x_1) dx_0 d\xi \tag{13}$$

where E' is the plain strain elastic modulus; x_0 is the position of measuring the COD; x_1 is the location where the unit dipole force is applied; ξ is the variable crack length. The same approach is used to calculate the COD owing to the drawing stress σ_{dr} as follows:

$$\delta_{int,ext}^{dr} = -\frac{2\sigma_{dr}}{E'} \int_x^{L} \int_{l_{CR}}^{\xi} G_{int,ext}^{SIF}(\xi, R_o, R_i, x_0) \cdot G_{int,ext}^{SIF}(\xi, R_o, R_i, x_1) dx_0 d\xi \tag{14}$$

The total COD δ_{tot} is found by the superposition of the COD due to internal pressure P_i and the drawing stress σ_{dr}. Hence, δ_{tot} is calculated by the following equation $\delta_{tot} = \delta_{\infty} + \delta_{dr}$. The GF for a butt-fusion welded pipe induced circumferential crack is discussed next.

3.4. Substitute geometry Green's function for the butt-fusion joint

For highly critical pipe applications and key structural components, it is important to generate specific GFs for the exact crack geometry. Existing GFs for simple geometries can, in fact, be used for the more complicated ones, based on the concept of "substitute geometry" or equivalent geometry" resulting in a wider-ranging practical applications (Wu & Xu, 2022). Such concept has been adopted by various industries for fracture mechanics analyses of complex structures (Zerbst et al., 2005). This would only require the stress field $\sigma(\xi)$ of the un-cracked component which can be generated using the finite element methods (FEM), thus making the method very general. With that, the application range of the CL theory can be greatly expanded.

The basic idea is to use the GF of either the internal or external pipe circumferential crack for the more complex butt-fusion welded pipe geometry. It should be emphasized, however, that the two geometries must be quite similar. Since $G_{int,ext}^{SIF}$ for a pipe circumferential crack is known, only the crack line stress for the butt-fusion joint needs to be determined. Nevertheless, it should be noted that the GFs determined using this approach are typically higher than the ones from the rigorous methods, which makes the analysis rather conservative. Two key cases are developed in this work, one is for a pipe butt-fusion joint weld center (WC) crack and another for a weld edge (WE) crack. Accordingly, the normalized stress line $\sigma(\xi)/\sigma_0$ profiles along the presumed crack line were generated using FEM for a weld edge crack, as shown in Fig. 5a, and a weld center crack, as displayed in Fig. 5b.

The stress output profiles are then fitted to exponential functions with variable positions x against the pipe wall, as per the following equation:

$$f_{WE,WC}\left(\frac{x}{W}\right) = Ae^{-\lambda(x/W)} + B \tag{15}$$

where A, λ and B are varying parameters of the function. The respective weld edge function, f_{WE}, parameters and weld center, f_{WC}, ones are listed in Table 5. The resulting plots in Fig. 5c and 5d display the FEA output and the exponential fit. With that, SIF Green's function for the collective butt-fusion welded pipe induced circumferential crack, displayed in Fig. 5e and 5f, can be constructed for the respective case, as follows:

$$G_{WE}^{SIF}(L, R_o, R_i; x, \xi) = \frac{\sigma_{int,ext}^{WE}(\xi)}{\sigma_0} \cdot G_{int,ext}^{SIF}(L, R_o, R_i; x) \tag{16}$$

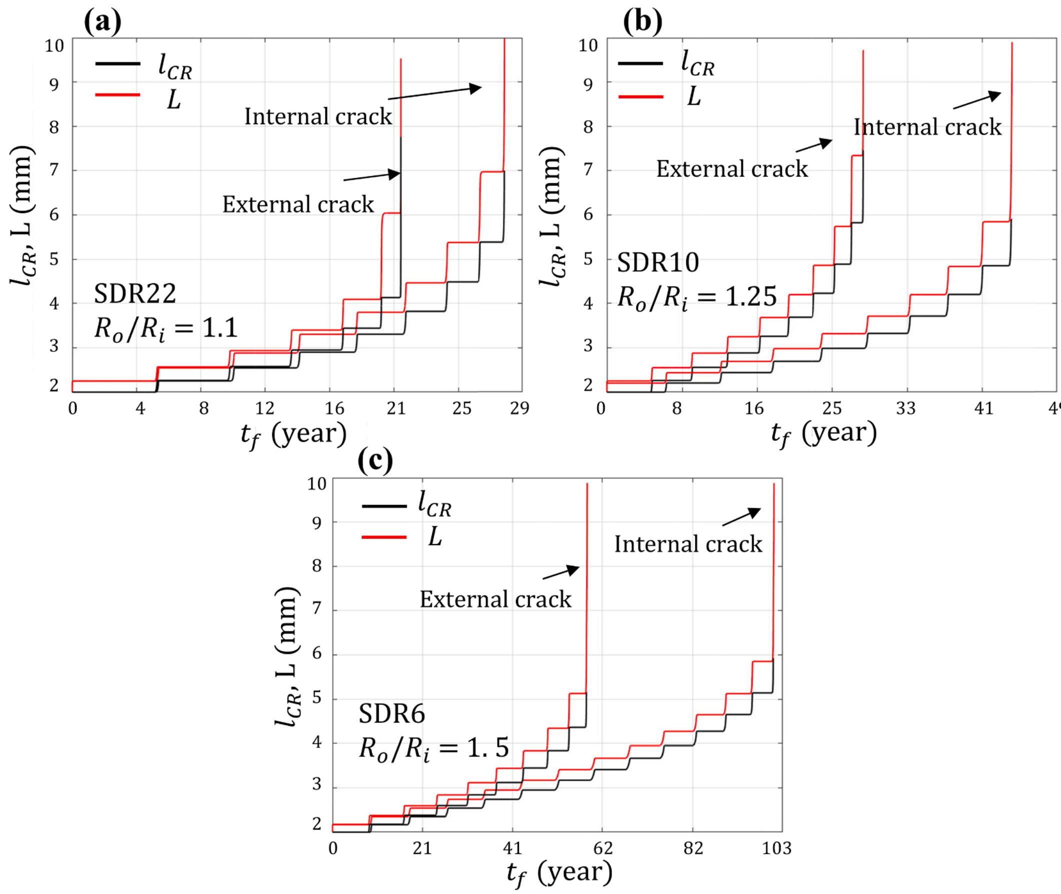

Fig. 9. The crack and CL system growth simulation versus the elapsed time of a pressurized pipe under nominal axial stress $P_iR_i/2W = 6.0$ MPa, for (a) SDR22; (b) SDR10; (c) SDR6. (For interpretation of the references to color in this figure legend, the reader is referred to the web version of this paper.).

$$G_{WC}^{SIF}(L, R_o, R_i; x, \xi) = \frac{\sigma_{int,ext}^{WC}(\xi)}{\sigma_0} \cdot G_{int,ext}^{SIF}(L, R_o, R_i; x)$$

where $\sigma_{int,ext}^{WE}(\xi)$ and $\sigma_{int,ext}^{WC}(\xi)$ denote the weld edge and weld center FEM generated crack line stresses of the un-cracked pipe; σ_0 is the normalizing stress value. Next, the TFs for the crack and PZ growth can be determined for a specified internal pressure *Pi*. Within the butt-fusion joint, an inhomogeneous behavior can induce unique micro-mechanical properties along the various regions. Such influence and its incorporation in the CL constative equations will be explained next.

3.5. Material inhomogeneity in the butt-fusion joint

Fig. 6a illustrates a cross-section of a butt-fusion joint produced from HDPE pipe and subjected to mild heat-reversion (Shaheer et al., 2017). The HDPE butt-fusion joint can be seen with distinct manifestations of structural orientation within the inner center region, i.e., melt flow zone (MFZ), displayed in Fig. 6a. The MFZ is unique with the coexistence of oriented and isotropic crystalline structure. Within the MFZ, the chains consist of both ones perpendicular to the pressure direction, and ones oriented along the various regions of the MFZ, as shown in Fig. 6b. In the center lies the plane of co-crystallization across which the faces of the two pipe ends molecularly entanglement which is primarily driven by thermal mobility and contact diffusion.

Under axial pressure, the hot mobile molecules on each pipe end, across this radially stretched plane, come into close contact wherein the molecular van der Waals' force pull the molecules from each planes together. This triggers the solidification process which advances forward to the plane of co-crystallization induced by the thermal conduction of the pipe taking away the heat from the MFZ. When the temperature decreases below HDPE crystallization temperature, the molecular diffusion stops, and the solidification process ends.

The HDPE butt-fusion joint SCG resistance is greatly influenced by the number of molecules which diffuse across the fusion planes. As the effective molecular crossings increases, the longer the molecule penetrates the interface. This consequently enhances the butt-joint resistance to SCG and fracture. This, consequently, can develop a heterogenous micro-mechanical behavior manifested by a non-uniform elastic modulus E within and adjacent to the MFZ, as outlined in Fig. 6c. Therefore, hardness measurements via nanoindentation suggests that the influence of heat dissipation from the MFZ extends much further into the parent material. The variation, however, is limited to approximately 7 % at the weld center (WC) E_{WC}, and to nearly 4 % at the weld edge (WE) E_{WE}, as shown in Fig. 6d (Veselý et al., 2009). The relevant Elastic Modulus E_i, listed in Table 6 will be used for the corresponding crack position across the butt-joint, e.g., WE, or WC. Next, the simulation algorithm of the CL model will be discussed.

3.6. Simulation algorithm of the CL model

As for the SFE, denoted as 2γ, it is expected to decrease with time at the crack tip. Depending on the environment, this degradation can be mechanical, chemical and at times both. The of the PZ degradation is assumed to follow a creep damage, i.e., time-dependent deformation, that takes place within the drawn ligaments. By neglecting any dependency for the PZ state on its deformation history, the SFE reduction process can be expressed as $\gamma(t, t_x) = \gamma_0\omega(t - t_x)$ (Chudnovsky & Shulkin, 1999). Where ω is a function that decreases with time. With that, the PZ creep deformation can be reflected by defining the function ω as $\omega = \Omega(t - t_x)^{-1}$, where Ω represents a creep function for the ligaments. The

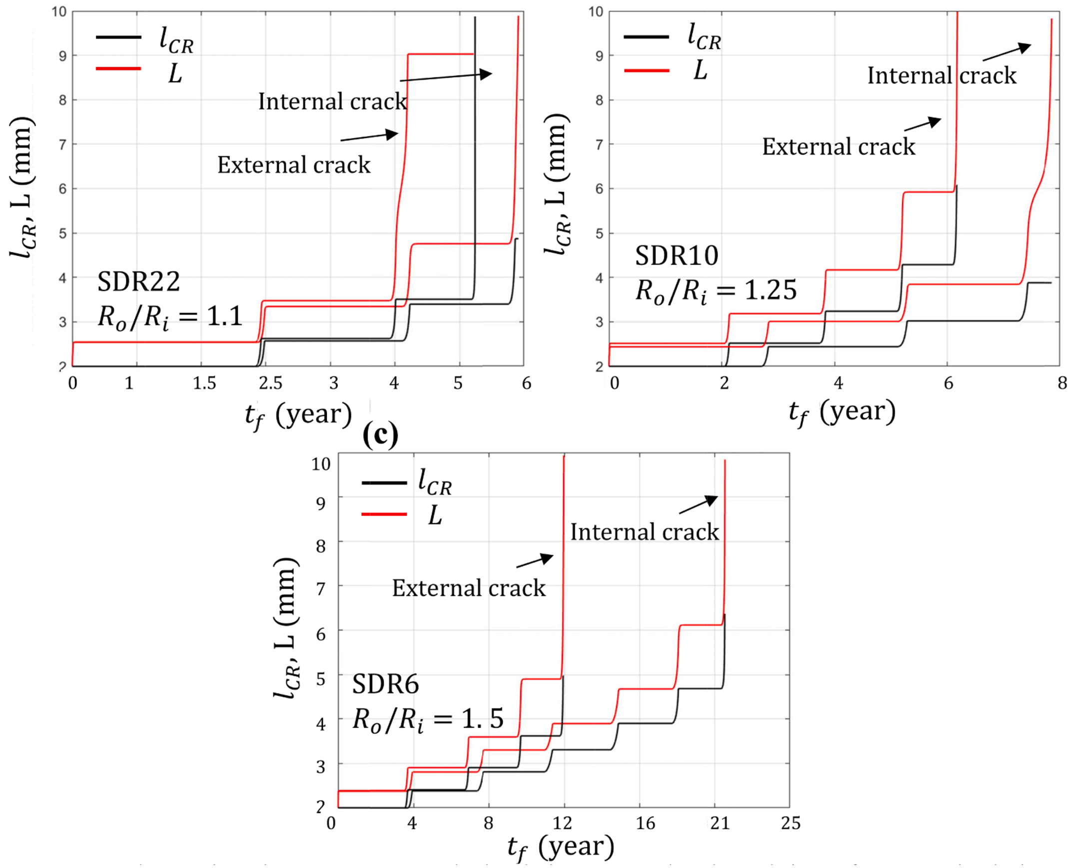

Fig. 10. The crack and CL system growth simulation versus the elapsed time of a pressurized pipe under nominal axial stress $P_iR_i/2W = 9.0$ MPa, for (a) SDR22; (b) SDR10; (c) SDR6. (For interpretation of the references to color in this figure legend, the reader is referred to the web version of this paper.).

Table 7
The input parameters of the discontinuous CL growth simulations in Figs. 8-10.

Description	Symbol	Unit	Value
Nominal axial stress	$P_iR_i/2W$	MPa	4.5, 6.0, 9.0
Pipe wall thickness	W	mm	10
Initial crack length	a	mm	2
Standard dimension ratio	SDR	–	22, 10, 6
Drawing stress	σ_{dr}	MPa	15
Plane strain elastic modulus	E'	MPa	1000
Natural drawing ratio	λ	–	6
Transformation energy per unit volume	γ^{tr}	mJ/mm^3	7
Initial surface fracture energy	γ_0	mJ/mm^2	15
Characteristic time	t^*	h	400

simplest expression in which the process of PZ degradation can be reflected is $\Omega = 1 + (t - t_x)/t^*$, with t^* being a characteristic time for the drawn fibers. The mechanical decay expression of the SFE used is as follows:

$$2\gamma(x,t) = 2\gamma_0 \bullet \frac{1}{1 + \frac{t_i - t_x}{t^*}} \tag{17}$$

where $2\gamma_0$ is undamaged material SFE, t^* is a characteristic time that controls the SFE degradation rate, and t_x is the time of materials transformation at the point x calculated based on l_{CR} position with respect to l_{PZ}. The characteristic time, t^*, follows an Arrhenius type equation, $t^* = t_0 \exp(-J/RT)$ and strongly depends on temperature, where t_0 is a time scale, J is the activation energy of the process, R is the universal gas constant and T is temperature in Kelvin. The larger the t^* is, the slower the decay inside the PZ. In order to achieve a new thermodynamic equilibrium configuration, the PZ grows until the crack driving force is negative. In discontinuous SCG, the ERR is lower than the initial SFE which would result in a negative crack driving force, i.e., no crack advancement and a stationary state takes place. As degradation progresses, the crack driving force becomes positive and consequently the crack grows. Once a new material is encountered, the crack arrests with a high initial SFE. Therefore, the previous crack jump length can be analogous to the stable PZ length and a stick–slip mechanism is observed. As long as the driving forces are positive, the following relationships are employed:

$$\dot{\ell}_{CR} = k_{CR}X^{CR}; \dot{\ell}_{PZ} = k_{PZ}X^{PZ} \tag{18}$$

where $\dot{\ell}_{CR}$ and $\dot{\ell}_{PZ}$ are the crack and PZ growth rates, respectively. Meanwhile, k_{CR} and k_{PZ} are the crack and the PZ kinetic coefficients. Once the CL is in equilibrium, the forces drop to zero and no growth takes place. The equations, despite their simple appearance, are nonlinear systems and require numerical solvers. The latter is discussed in the next section. The crack keeps on growing until a local instability occurs and the SCG transforms to RCP.

The algorithm of the CL system simulation is primarily made based on a loop statement along with multiple stages that dictate a single loop of calculation. For the i-th loop, the length of the crack $l_{CR}(i+1)$ and crack layer $L(i+1)$ are calculated using the following equations for a selected time increment Δt:

$$\begin{cases} l_{CR}(i+1) = l_{CR}(i) + \dot{l}_{CR}(i) \bullet \Delta t \\ L(i+1) = L(i) + \dot{L}(i) \bullet \Delta t, \end{cases} \tag{19}$$

The crack and PZ evolution are calculated using Eqs. (19). In the 1st stage of the loop, the initial SFE and the crack tip SFE are equal. Using the superposition method, the ERR $J_1^{PZ}(i)$, and the COD $\delta_\infty(i)$ at the PZ are calculated. The corresponding lengths would only change if the

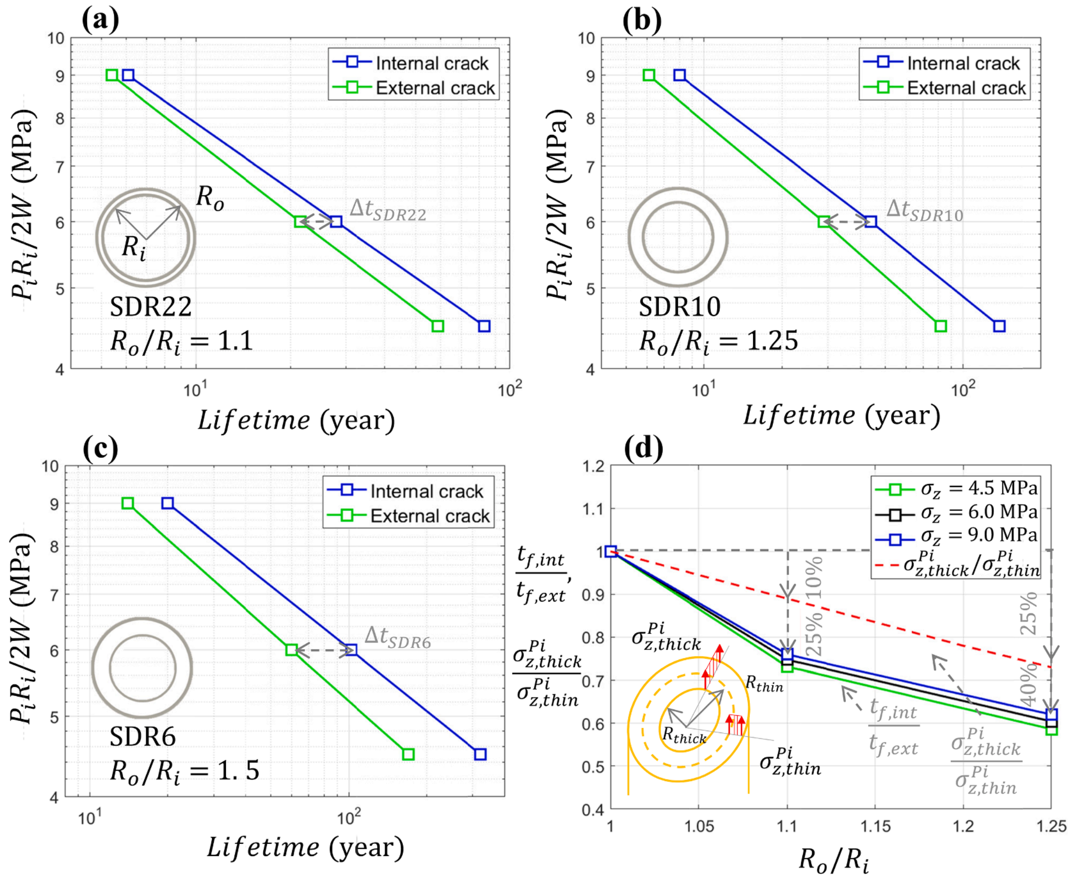

Fig. 11. Nominal axial stress $P_iR_i/2W$ against t_f for an internal and external circumferential pipe crack for (a) SDR 22, (b) SDR 10, (c) SDR 6. (d) Lifetime and axial stress ratios against various R_o/R_i ratios under internal pressure P_i. (For interpretation of the references to color in this figure legend, the reader is referred to the web version of this paper.).

Table 8
The CL material and physical input parameters for HDPE at different temperatures.

Description	Symbol	Unit	Typical value		
			$T = 23$ °C	$T = 60$ °C	$T = 80$ °C
Drawing stress	σ_{dr}	MPa	17	10	7.5
Transformation energy per unit volume	γ^{tr}	mJ/mm^3	40	17	7
Initial surface fracture energy	γ_0	mJ/mm^2	20	15	10
Natural drawing ratio	λ	–	4	5	6
Plane strain elastic modulus	E'	MPa	700	500	250
Characteristic time	t^*	h	600	60	20

driving forces were positive. In the 2nd stage of the loop, ‘i + 1′-th loop, the crack tip SFE $\gamma(i+1)$ would change based on the numerical code, illustrated in Fig. 3. For example, if the new crack length $l_{CR}(i+1)$ was in between $l_{PZ}(i-2) \le l_{CR}(i+1) < l_{PZ}(i-1)$, the SFE would be $\gamma_0 \bullet f(3dt)$. Similarly, if the new crack length was instead in between $l_{PZ}(i) \le l_{CR}(i+1) < l_{PZ}(i+1)$, the SFE would be $\gamma_0 \bullet f(dt)$. Finally, if the new crack and PZ lengths are equal $l_{CR}(i+1) = l_{PZ}(i+1)$, the SFE goes back to the initial SFE $\gamma(i+1) = \gamma_0 \bullet f(0)$ whereby a fresh material is encountered.

In order to relate the physical SCG process in a pipe induced by a circumferential crack l_{CR} and the crack layer L, the CL discontinuous SCG mechanism under internal pressure P_i is outlined in Fig. 7. The time elapsed from the test is denoted t. At $t = 0$, the crack length is a_0, meanwhile the PZ develops at the crack tip. The crack would only grow if the ERR at the tip is larger than the initial SFE γ_0. Ultimately, the PZ reaches equilibrium, as shown at t_2. The PZ keeps on decaying with the generated axial stress σ_z^{Pi}, which lead to the crack penetrating the PZ area, as displayed at t_3 to t_5. Simultaneously, the PZ size increases, while the crack advances. The second arrest starts, accordingly, for the next jump at t_5. In essence, the arrest cycles represent the time needed for sufficient PZ decay.

In the 3rd stage of the algorithm, two instability or failure criterion are used for terminating the simulation. The 1st being the SIF exceeding the material fracture toughness, K_{Ic}. The 2nd being the remaining ligament exceeding the pipe wall thickness, W. Finally, once failure takes place, the crack l_{CR} and crack layer l lengths are plotted against time-to-failure t_f, as displayed in the output graph of Fig. 7. With that, the entire CL history can be seen. The proposed CL model output is discussed next including the discontinuous SCG simulations of pipe and butt-fusion joints induced cracks.

4. Results and discussion

4.1. Circumferential crack simulations for various SDRs and internal pressures

Discontinuous SCG were simulated for three SDRs, i.e., 22, 10 and 6, and internal pressures P_i, as shown in Figs. 8-10, for both an internal and an external circumferential pipe crack. The initial crack length chosen was 0.2 W, whereby W is the pipe wall thickness. The applied nominal axial stress against the pipe wall, $P_iR_i/2W$, were 4.5, 6.0, and 9.0 MPa. The material and geometric parameters used in the CL simulations are listed in Table 7. The lifetime t_f of the internal circumferential crack,

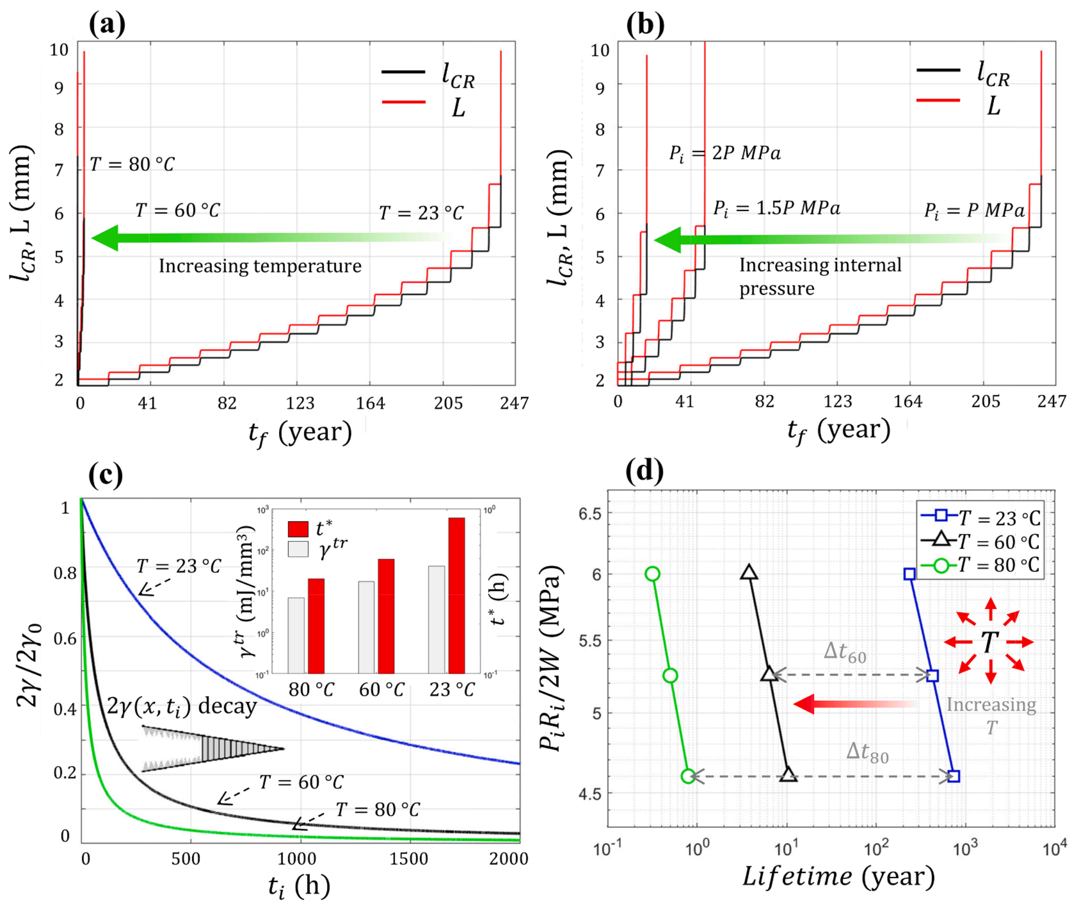

Fig. 12. CL simulations of a pressurized HDPE pipe with a 0.2 W external circumferential crack at (a) multiple temperatures of T = 23 °C, 60 °C, and 80 °C, (b) at multiple pressures of $PMPa, 1.5PMPa, and 2P MPa$. (c) The surface fracture energy 2γ decay rates against the degradation time at the respective temperature, including the characteristic time t^* and PZ transformation energy density γ^{tr}. (d) Effect of temperature on the cracked pipe lifetime t_f at several nominal axial stress $P_iR_i/2W$ levels.

across all the generated simulations, was longer than the external crack. The latter is explained by the variation of the SIF from Green's functions $G^{SIF}_{int,ext}$ being higher at the pipe outer wall, which was also reported by Fakhri et al. (Fakhri et al., 2019) and Li et al. (Li et al., 2020). This faster growth was, as well, observed by Olamide et al. (Olamide et al., 2020), and indicates the need for an earlier assessment for external cracks compared to internal ones. This is contrary to the case of longitudinal cracks, whereby t_f of an external crack was found larger, justified by the hoop stress distribution $\sigma^{Pi}_{\theta}(x)$ being higher at pipe inner wall (Wee, Park, et al., 2020).

The observed difference in t_f between the external and internal circumferential crack, on the other hand, was seen to diminish the larger the SDR, i.e., the thinner the pipe. For instance, the difference in t_f for SDR 22 is approximately 25 % for $P_iR_i/2W$ of 6.0 MPa, while it increased to 45 % for SDR 6, i.e., the thickest pipe. This can also be seen in the log–log plot of the nominal axial stress $P_iR_i/2W$ against failure time t_f for the three SDRs, shown in Fig. 11a-11c, with larger differences between t_f the smaller the SDR, i.e., $\Delta t_{SDR6} > \Delta t_{SDR10} > \Delta t_{SDR22}$. In addition, the higher the internal pressure P_i, the shorter the crack arrest time and larger SCG step jumps observed, which results in a decreased failure time t_f. Similar CL growth kinetics observed herein from P_i was seen in previous studies by Wee et al. (Wee & Choi, 2016; Wee, Park, et al., 2020) against the level of applied load, which in all cases led to an acceleration in the SCG propagation behavior.

In order to assess the influence of the SDR on the internal crack failure time $t_{f,int}$ and the external crack $t_{f,ext}$ more thoroughly, their ratio $t_{f,int}/t_{f,ext}$ against R_o/R_i is plotted in Fig. 11d. The axial stress ratio of thick to thin-walled pipes $\sigma^{Pi}_{z,thick}/\sigma^{Pi}_{z,thin}$ is also plotted in the same figure. The uncracked thick-walled to thin-walled pipe internal pressure P_i induced axial stress σ^{Pi}_{z} is generated. It can be seen that $t_{f,int}/t_{f,ext}$ decreases the higher the R_o/R_i and hence the smaller the SDR, i.e., thicker pipe. This effect is observed regardless the P_i value, implying that Fig. 11d can be a master curve for $t_{f,int}/t_{f,ext}$. Overall, pipes with SDR > 20 are considered thin walled with a constant hoop stress of $\sigma^{Pi}_{\theta} = P_iR_i/W$, owing to the difference in stress surfaces being < 10 %. Under such conditions, the inner and outer circumferential crack can be evaluated equally. Nevertheless, and interestingly, this difference for HDPE discontinuous SCG t_f can be doubled, i.e., 25 %, for SDR 22 and 40 % for SDR 6, as shown in the dashed arrows in Fig. 11d. Therefore, the lifetime predictions of even thin-walled cracked HDPE pipes should be evaluated more carefully.

4.2. Circumferential crack simulations for various temperatures

At elevated temperatures, e.g., T = 80 °C and 60 °C, the CL growth appears with relatively faster propagations between the AZ stationary configurations. The jump length manifested by the distances between the fracture surface striations increases. Such temperatures trigger thermally activated chain sliding processes which accelerates the molecular mobility and consequently the rupture of the PZ fibrils, i.e., the transition from the material continuum media to highly drawn membranes. That is, less energy for a unit volume transformation into PZ γ^{tr} would be required, i.e., lower cold drawing resistance near the crack tip. However, the stepwise crack growth mechanism doesn't change and the

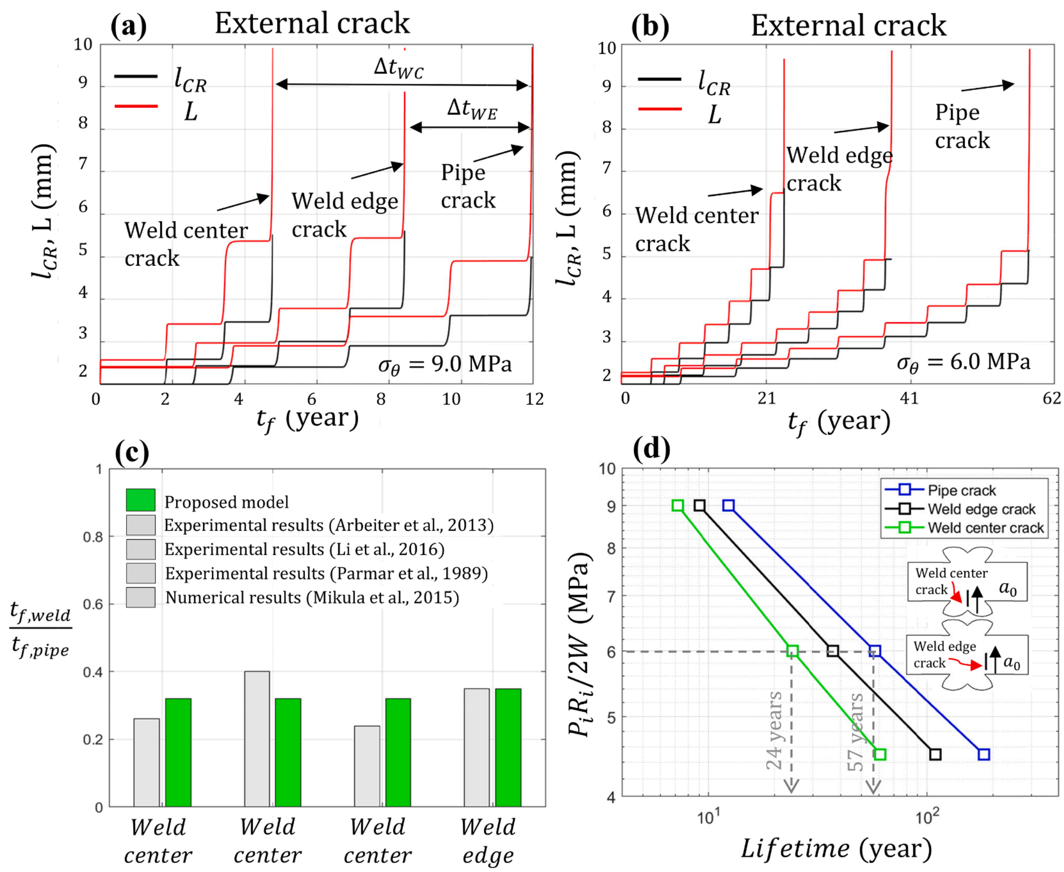

Fig. 13. Discontinuous CL simulations of a pressurized HDPE pipe with a 0.2 W circumferential crack initiating from the pipe, weld edge and weld center under nominal axial stress $P_iR_i/2W$ of (a) 9.0 MPa, and (b) 6.0 MPa. (c) The CL model first weld to pipe failure time ratio $t_{f,weld}/t_{f,pipe}$ compared with the results of the previous studies. (d) Effect of nominal axial stress $P_iR_i/2W$ on the lifetime t_f variation of a pipe crack, weld center crack, and a weld edge crack. (For interpretation of the references to color in this figure legend, the reader is referred to the web version of this paper.).

crack advances through a discontinuous SCG mode.

The basic approach to generate the CL simulations at various temperatures is to acquire the material and physical properties entering the thermodynamic forces of the CL model, at the desired temperature. The latter includes the drawing stress σ_{dr}, the transformation energy per unit volume γ^{tr}, the initial surface fracture energy γ_0, the natural drawing ratio λ, and the plane strain elastic modulus E'. Such parameters have been collected from previous studies for HDPE at T = 23 °C, 60 °C, and 80 °C (Chudnovsky et al., 2012; Shahin et al., 2020; Wee, Park, et al., 2020). It has to be emphasized, however, that the room temperature transformation energy γ^{tr} is an extrapolated value through the use of the Arrhenius technique from Chudnovsky et al. (Chudnovsky et al., 2012). Nonetheless, the rate of γ^{tr} which dictates the SFE decay of the PZ is controlled by the characteristic time t^*. The CL material and physical input parameters employed in the simulations are listed in Table 8.

Discontinuous SCG were simulated for a HDPE pipe with external circumferential crack of initial length 0.2 W, and SDR 6. Fig. 12a shows the SCG simulations for a nominal axial stress $P_iR_i/2W$ of 6.0 MPa at T = 23 °C, 60 °C, and 80 °C. Whereas Fig. 12b displays the CL simulations at T = 23 °C for three internal pressure levels of P_i, 1.5 x P_i, and 2 x P_i, whereby P_i generates a σ_z^{Pi} of 6.0 MPa. It can be observed that temperature T decreased the pipe lifetime t_f significantly higher than the internal pressure P_i. At the same time, while a 50 % increase in P_i decreased the failure time t_f approximately 75 %, subjecting the pipe to a constant temperature of 60 °C dropped t_f by almost 95 % of its original lifetime. A similar exponential drop with > 95 % in t_f was reported by Kalyanam et al. (Kalyanam et al., 2015) using a circumferentially cracked HDPE pipe under internal pressure P_i, at 23 °C and 80 °C. Fig. 12d demonstrate the effect of temperature on a log–log scale, which shows a clear logarithmic shift in the pipe lifetime from 23 °C to 80 °C. A larger variation in t_f is observed at 60 °C compared to 80 °C with Δt_{80} less than twice Δt_{60}. This highlights the non-linearity of the curves shift and the due care required in evaluating the pipe remaining life at elevated temperatures.

4.3. *Butt-joint crack simulations for various positions and internal pressures*

The SCG resistance of butt-fusion joints is substantially lower than that of a parent pipe, even when the short-term tensile strengths are comparable. Compared to the weld edge, the developed joint interface owing to the macromolecular kinetics during the welding process results in the weld center being the weakest. Such variation in the life expectancy between a pipe crack and a butt joint crack has been demonstrated by several past studies whether experimentally by Arbeiter et al. (Arbeiter et al., 2013), Parmer et al. (Parmar & Bowman, 1989), and Li et al. (Li et al., 2016), or numerically by Mikula et al. (Mikula et al., 2015). Although the drop in lifetime was found with scatter, it was always seen leading to a significant decrease in the pipe failure time t_f.

Figs. 13a and 13b show the discontinuous SCG simulations induced by (1) a pipe circumferential crack, (2) a weld-edge circumferential crack, and (3) weld center crack, at $P_iR_i/2W$ of 9.0 MPa and 6.0 MPa. A SDR 6 pipe with an initial crack length of 0.2 W under the combined action from axial stress σ_z^{Pi} and the weld geometry stress field $\sigma(\xi)$ was chosen. Different elastic moduli for the respective crack location, as listed in Table 6, were used. The lifetime t_f, across all the generated simulations, was longer for pipe crack, followed by the weld edge crack

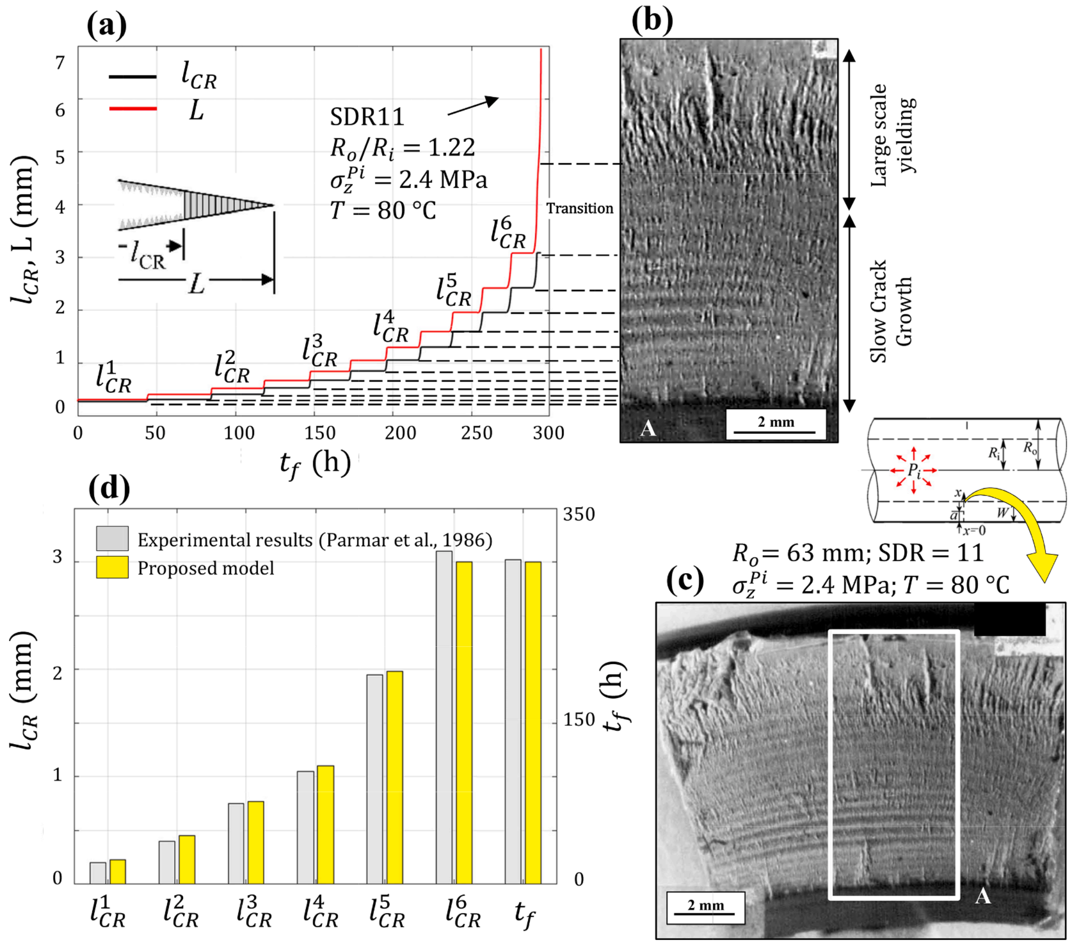

Fig. 14. Comparison of the CL proposed model (a) simulation with (b) the experiments magnified fracture surface from (c) for a 63 mm polyethylene pipe of SDR 11, at $\sigma_z = 2.4$ MPa, and T = 80°C. (d) The CL model first five steps l^1_{CR} till l^5_{CR}, and total failure time t_f compared with the results of the experiment. The experimental results were
adopted from Parmar et al. (Parmar, 1986).

then the weld center crack. The simulation results were compared with the experimental and numerical results of several scholars, as displayed in Fig. 13c. The ratio of weld failure time $t_{f,weld}$ to the pipe failure time $t_{f,pipe}$ was used as a measure of t_f variation induced by the butt-fusion joint $\sigma(\xi)$. It can be seen, that proposed model $t_{f,weld}/t_{f,pipe}$ is consistent with majority of the previous works. However, it must be emphasized, that the chosen weld beads shape, size, and profile can have a significant influence on the joint stress field distribution $\sigma(\xi)$ along the presumed crack line. Thus, due care should be taken in mimicking the butt-fusion joint profile for simulation accuracy.

The effect of axial stress $P_iR_i/2W$ on each of the pipe crack, weld center crack and weld edge crack lifetime t_f is shown in Fig. 13d. Although the relationships on the log–log scale is found linear, the higher the internal pressure P_i, the larger the difference in t_f, represented by Δt_{WC} for weld center cracks and Δt_{WE} for weld edge cracks. It also indicates that a weld center crack would fail to guarantee the HDPE pipe 50 years life expectancy and only sustain 24 years. Overall, the suggested modified pipe butt-fusion CL model can theoretically simulate the joint induced drop in lifetime t_f including the unique discontinuous SCG kinetics of HDPE with considerable accuracy. A comparison of the developed pipe circumferential CL with experiments fracture surfaces is discussed next.

5. Comparison of the developed model with experiments

In this section, the proposed CL model is used on a HDPE pipe with an outside diameter R_o of 63 mm, SDR 11 and a circumferential crack of 0.08 W. The pipe is subjected to a nominal axial stress $P_iR_i/2W$ of 2.4 MPa due to the internal pressure P_i, and is pressurized at T = 80 °C. Parmer et al. (Parmar, 1986), reported experimental results on the internal pressure fatigue testing of butt-fusion welded polyethylene pipes where discontinuous SCG behavior was observed. The internal pressure P_i was cycled between 0-gauge pressure and 9.5 bar giving a stress ratio $R(\sigma_{min}/\sigma_{max}) = 0$, and a nominal axial stress $P_iR_i/2W$ of 2.4 MPa. The test was carried out at T = 80 °C with an initial notch located at the weld bead. These conditions were chosen to provoke a quasi-brittle discontinuous SCG mode. The test frequency f applied was kept at 0.083 Hz which can represent typical pressure surges in water distribution networks.

Fig. 14a shows the CL simulations of the developed model. The red and black curves represent the CL length L and the crack length l_{CR}, respectively. Fig. 14b, on the other hand, displays a magnified view of the fracture surface of the experimental P_i fatigue tested pipe butt-weld from the full surface in Fig. 14c. It can be observed that the discontinuous SCG kinetics were successfully simulated. The CL model results were quantitatively compared with the experimental results in terms of the crack length in the first five steps l_{CR}^1 till l_{CR}^5, and total failure time t_f, as shown in Fig. 14a. As shown in Fig. 14d, the proposed model is highly consistent with the experimental results for l_{CR}^1 till l_{CR}^5 including t_f, respectively. Hence, the proposed CL model with the appropriate material parameters can theoretically simulate the pipe butt-fusion induced circumferential SCG as well as the unique discontinuous kinetics of HDPE with considerable accuracy.

6. Conclusions

In this work, a SCG model based on the CL theory for HDPE pipes circumferential and butt-fusion joints induced cracks was developed. A SCG model for pipes with circumferential internal and external cracks for multiple standard dimension ratios, i.e., $6 \leq \text{SDR} \leq 22$ was formulated. The proposed CL model was also extended to butt-fusion edge and center-line induced pipe cracks. Lastly, the CL simulations were compared with experimental discontinuous SCG results from HDPE pressurized pipes.

In summary, pipes and butt-fusion circumferential cracks thermodynamic forces (TFs) for the crack and PZ growth were constructed. The required Green's functions based on the concept of "substitute geometry" were developed. A fundamental framework for the CL model is established, following the 'equivalent geometry' approach. Subsequently, a CL simulation algorithm was introduced based on a time-marching loop. Further, a parametric study on the influence of SDR, internal pressure P_i, and temperature on the lifetime variation of internally and externally cracked HDPE pipes was conducted.

Unlike longitudinal cracks, the lifetime t_f of external circumferential cracks were found shorter than the internal ones, mandating an earlier assessment. Pipes with SDR > 20 that are considered thin walled with a constant hoop stress σ_θ^{Pi} were found with $t_{f,int}/t_{f,ext}$ of > 20 %. This difference for HDPE discontinuous SCG t_f was found to even reach 40 % for SDR 6. The latter implies that the lifetime predictions of even thin-walled cracked HDPE pipes should be evaluated with a more conservative criterion. Discontinuous crack jumps l_{CR} and total failure time t_f of butt-fusion welded and circumferentially cracked HDPE pipes were simulated with considerable accuracy.

Overall, this study aims to extend the applicability of the CL theory to highly critical applications such as the butt joints of pressurized HDPE pipes. The outcomes of this work also aid in expanding the theory's implementation in many industrial and design applications, enabling the use of HDPE pipes with improved reliability. A similar approach can be followed for other complex geometries which lay the basis for establishing a procedure for the CL theory implementation. In the future, additional investigation is needed on the effect of hoop stress σ_θ^{Pi} on the crack driving force along with the axial stress σ_z^{Pi}. This simplification is typically conservative. For that, examining the impact of the stress parallel to the crack front can be a future direction, in attempt to investigate this biaxial loading effect.

In the future, additional investigations can be done in order to improve the developed CL model. For example: 1) a dedicated theoretical formalism with a comparison between open profile, i.e., corrugated outer wall, and closed profile, i.e., smooth outer wall, can be a future research direction. Such corrugated PE pipes are mostly buried requiring the incorporation of soil models, would be key. 2) Some pipelines are used in harsh and cold environments, e.g., northern climate, submarine pipeline. For that, acquiring the material and physical properties entering the thermodynamic forces of the CL model, at such low temperatures would aid in expanding the model applicability.

Declaration of competing interest

The authors declare that they have no known competing financial interests or personal relationships that could have appeared to influence the work reported in this paper.

Acknowledgement

The authors would like to acknowledge UAE University for providing the facilities and funds through Materials library (#31N392) - Industry 4.0 district project.

References

Allwood, W.J., Beech, S.H., 1993. The development of the 'notched pipe test' for the assessment of the slow crack growth resistance of polyethylene pipe [Article]. Constr. Build. Mater. 7 (3), 157–162. https://doi.org/10.1016/0950-0618(93)90053-F.

Almomani, A., Deveci, S., Mourad, A.-H.-I., Barsoum, I., 2022. Constitutive model calibration for the thermal viscoelastic-viscoplastic behavior of high density polyethylene under monotonic and cyclic loading. Polym. Test. 107911.

Almomani, A., Mourad, A.-H.-I., 2023. The fracture toughness of Schwarz Primitive triply periodic minimal surface lattice. Theor. Appl. Fract. Mech. 125, 103924.

Almomani, A., Mourad, A.-H.-I., Deveci, S., Wee, J.-W., Choi, B.-H., 2023. Recent advances in slow crack growth modeling of polyethylene materials. Mater. Des. 111720.

Almomani, A., Mourad, A.-H.-I., Deveci, S., 2024. Effect of the crack layer theory parameters on the discontinuous slow crack growth of high density polyethylene under fatigue loading. Int. J. Solids Struct. 286, 112579.

Arbeiter, F., Pinter, G., & Frank, A. (2013). Impact of single and dual pressure butt-welding procedures on the reliability of PE 100 pipe welds. In *Proceedings of Eurotec 2013*.

Balika, W., Pinter, G., Lang, R.W., 2007. Systematic investigations of fatigue crack growth behavior of a PE-HD pipe grade in through-thickness direction [Article]. J. Appl. Polym. Sci. 103 (3), 1745–1758. https://doi.org/10.1002/app.25073.

Barton, N.A., Farewell, T.S., Hallett, S.H., Acland, T.F., 2019. Improving pipe failure predictions: Factors affecting pipe failure in drinking water networks. Water Res. 164, 114926.

Benhamena, A., Bachir Bouiadjra, B., Amrouche, A., Mesmacque, G., Benseddiq, N., Benguediab, M., 2010. Three finite element analysis of semi-elliptical crack in high density poly-ethylene pipe subjected to internal pressure [Article]. Mater. Des. 31 (6), 3038–3043. https://doi.org/10.1016/j.matdes.2010.01.029.

Benhamena, A., Aminallah, L., Bouiadjra, B.B., Benguediab, M., Amrouche, A., Benseddiq, N., 2011. J integral solution for semi-elliptical surface crack in high density poly-ethylene pipe under bending [Article]. Mater. Des. 32 (5), 2561–2569. https://doi.org/10.1016/j.matdes.2011.01.045.

Bergström, G., Nilsson, S., & Lindqvist, L. (2004). The influence from pipe surface, weld beads and protective skins on long term failure times for PE butt fusion joints. *Plastics Pipes XII*.

Bowman, J., Parmar, R., 1989. The importance of axial misalignment on the long term strength of polyethylene pipe butt fusion joints [Article]. Polym. Eng. Sci. 29 (19), 1406–1412. https://doi.org/10.1002/pen.760291912.

Byrne, N., Ghanei, S., Espinosa, S. M., & Neave, M. (2023). Influence of hydrogen on vintage polyethylene pipes: slow crack growth performance and material properties. *International Journal of Energy Research*, *2023*.

Carpinteri, A., Brighenti, R., Vantadori, S., 2003. Circumferentially notched pipe with an external surface crack under complex loading. Int. J. Mech. Sci. 45 (12), 1929–1947.

Choi, B.H., Balika, W., Chudnovsky, A., Pinter, G., Lang, R.W., 2009a. The use of crack layer theory to predict the lifetime of the fatigue crack growth of high density polyethylene. Polym. Eng. Sci. 49 (7), 1421–1428.

Choi, B.H., Balika, W., Chudnovsky, A., Pinter, G., Lang, R.W., 2009b. The use of crack layer theory to predict the lifetime of the fatigue crack growth of high density polyethylene [Article]. Polym. Eng. Sci. 49 (7), 1421–1428. https://doi.org/10.1002/pen.21436.

Chudnovsky, A., 2014. Slow crack growth, its modeling and crack-layer approach: A review [Article]. Int. J. Eng. Sci. 83, 6–41. https://doi.org/10.1016/j.ijengsci.2014.05.015.

Chudnovsky, A., Moet, A., 1985. Thermodynamics of translational crack layer propagation. J. Mater. Sci. 20 (2), 630–635.

Chudnovsky, A., Shulkin, Y., 1999. Application of the crack layer theory to modeling of slow crack growth in polyethylene [Article]. Int. J. Fract. 97 (1–4), 83–102. https://doi.org/10.1023/a:1018683624720.

Chudnovsky, A., Zhou, Z., Zhang, H., Sehanobish, K., 2012. Lifetime assessment of engineering thermoplastics. Int. J. Eng. Sci. 59, 108–139.

Chudnovsky, A. (1984). *Crack layer theory*. The Center.

Deblieck, R.A.C., Van Beek, D.J.M., Remerie, K., Ward, I.M., 2011. Failure mechanisms in polyolefines: The role of crazing, shear yielding and the entanglement network [Article]. Polymer 52 (14), 2979–2990. https://doi.org/10.1016/j.polymer.2011.03.055.

El-Bagory, T.M.A.A., Sallam, H.E.M., Younan, M.Y.A., 2021. Effect of loading rate and pipe wall thickness on the strength and toughness of welded and unwelded polyethylene pipes [Article]. J. Pressure Vessel Technol. Trans. ASME 143 (1), 011505. https://doi.org/10.1115/1.4047444.

Fakhri, O.M., Kareem, A.K., Ismail, A.E., Jamian, S., Nemah, M.N., 2019. Mode I SIFs for internal and external surface semi-elliptical crack located on a thin cylinder. Test Eng. Manage. 81, 586–596.

Favier, V., Giroud, T., Strijko, E., Hiver, J.M., G'Sell, C., Hellinckx, S., Goldberg, A., 2002. Slow crack propagation in polyethylene under fatigue at controlled stress intensity. Polymer 43 (4), 1375–1382.

Fischer, J., Freudenthaler, P.J., Bradler, P.R., Lang, R.W., 2019. Novel test system and test procedure for fatigue crack growth testing with cracked round bar (CRB) specimens [Article]. Polym. Test. 78, 105998 https://doi.org/10.1016/j.polymertesting.2019.105998.

Huang, Y., Wang, X., Duan, X., 2020. Evaluation of crack opening displacement of through-wall circumferential-cracked pipe using direct weight function method. Theor. Appl. Fract. Mech. 108, 102595.

Hutař, P., Ševčík, M., Náhlík, L., Pinter, G., Frank, A., Mitev, I., 2011. A numerical methodology for lifetime estimation of HDPE pressure pipes [Article]. Eng. Fract. Mech. 78 (17), 3049–3058. https://doi.org/10.1016/j.engfracmech.2011.09.001.

Iso, 2009. Polyolefin pipes for the conveyance of fluids — Determination of resistance to crack propagation — Test method for slow crack growth on notched pipes. In: ISO 13479. ISO, p. (pp. 9):.

ISO. (2012). Thermoplastics pipes for the conveyance of fluids — Determination of the slow cracking resistance of pipes and fittings using the Notched Ring Test (NRT). In *ISO 16479*: ISO.

ISO. (2015). Polyethylene (PE) materials for piping systems — Determination of resistance to slow crack growth under cyclic loading — Cracked Round Bar test method. In *ISO 18489*: ISO.

ISO. (2005). Notch tensile test to measure the resistance to slow crack growth of polyethylene materials for pipe and fitting products (PENT). In *ISO 16241*: ISO.

ISO. (2019). Plastics — Determination of environmental stress cracking (ESC) of polyethylene — Full-notch creep test (FNCT). In *ISO 16770*: ISO.

Jayadevan, K.R., Østby, E., Thaulow, C., 2004. Fracture response of pipelines subjected to large plastic deformation under tension. Int. J. Press. Vessel. Pip. 81 (9), 771–783.

Kadota, K., Chudnovsky, A., 1992. Constitutive equations of crack layer growth [Article]. Polym. Eng. Sci. 32 (16), 1097–1104. https://doi.org/10.1002/pen.760321607.

Kalyanam, S., Krishnaswamy, P., Hioe, Y., Shim, D.J., Focht, E., 2015. A fracture mechanics approach to service life prediction of HDPE fusion joints in nuclear applications [Article]. Plast. Eng. 71 (6), 40–45. https://doi.org/10.1002/j.1941-9635.2015.tb01376.x.

Kim, Y.-J., Huh, N.-S., Kim, Y.-J., 2002. Quantification of pressure-induced hoop stress effect on fracture analysis of circumferential through-wall cracked pipes. Eng. Fract. Mech. 69 (11), 1249–1267.

Kim, J.-S., Oh, Y.-J., Choi, S.-W., Jang, C., 2019. Investigation on the thermal butt fusion performance of the buried high density polyethylene piping in nuclear power plant. Nucl. Eng. Technol. 51 (4), 1142–1153.

Kim, I., Zhao, Y., Choi, B.H., Lee, J.M., Lee, K.S., 2013. Numerical analysis of asymmetric fatigue crack growth behaviors of circular notched bar specimen resulting from various geometric misalignments [Article]. Eng. Fract. Mech. 108, 50–64. https://doi.org/10.1016/j.engfracmech.2013.04.015.

Krishnaswamy, R.K., Lamborn, M.J., 2005. The influence of process history on the ductile failure of polyethylene pipes subject to continuous hydrostatic pressure [Article]. Adv. Polym. Tech. 24 (3), 226–232. https://doi.org/10.1002/adv.20044.

Lai, H., Fan, D., Liu, K., 2022. The Effect of Welding Defects on the Long-Term Performance of HDPE Pipes. Polymers 14 (19), 3936.

Laiarinandrasana, L., Devilliers, C., Oberti, S., Gaudichet, E., Fayolle, B., Lucatelli, J.M., 2011. Ring tests on high density polyethylene: Full investigation assisted by finite element modeling. Int. J. Press. Vessel. Pip. 88 (1), 1–10.

Lancioni, N., Parlapiano, M., Sgroi, M., Giorgi, L., Fusi, V., Darvini, G.,…Fatone, F. (2023). Polyethylene pipes exposed to chlorine dioxide in drinking water supply system: A critical review of degradation mechanisms and accelerated aging methods. *Water Research*, 120030.

Lang, R.W., Stern, A., Doerner, G., 1997. Applicability and limitations of current lifetime prediction models for thermoplastics pipes under internal pressure [Article]. Angew. Makromol. Chem. 247, 131–145. https://doi.org/10.1002/apmc.1997.052470109.

Lee, P.A., Kim, S., Stakenborghs, B., Suh, Y., Choi, S., 2022. Development of hydro-axial tension method for whole pipe butt-fusion joint tensile test. Polym. Test. 109, 107553.

Li, H., Gao, B., Dong, J., Fu, Y., 2016. Welding effect on crack growth behavior and lifetime assessment of PE pipes [Article]. Polym. Test. 52, 24–32. https://doi.org/10.1016/j.polymertesting.2016.03.024.

Li, Z., Jiang, X., Hopman, H., Zhu, L., Liu, Z., 2020. An investigation on the circumferential surface crack growth in steel pipes subjected to fatigue bending. Theor. Appl. Fract. Mech. 105, 102403.

Lu, X., Qian, R., Brown, N., Buczala, G., 1992. The effect of pressure and contaminants on slow crack growth in a butt fusion in a polyethylene gas pipe [Article]. J. Appl. Polym. Sci. 46 (8), 1417–1427. https://doi.org/10.1002/app.1992.070460812.

Maiti, S.K., Mourad, A.H., 1995a. Criterion for mixed mode stable crack growth—I. Three point bend geometry. Eng. Fract. Mech. 52 (2), 321–347.

Maiti, S.K., Mourad, A.H., 1995b. Criterion for mixed mode stable crack growth—II. Compact tension geometry with and without stiffener. Eng. Fract. Mech. 52 (2), 349–378.

Mikula, J., Hutař, P., Nezbedová, E., Lach, R., Arbeiter, F., Ševčík, M.,…Náhlík, L. (2015). On crack propagation in the welded polyolefin pipes with and without the presence of weld beads [Article]. *Materials and Design*, *87*, 95-104. https://doi.org/10.1016/j.matdes.2015.07.131.

Mikula, J., Hutař, P., Ševčík, M., Nezbedová, E., Lach, R., Grellmann, W., Náhlík, L., 2017. Influence of Different Welding Conditions of Polyolefin Pipes on Creep Crack Growth. Deformation Fract. Behav. Polym. Mater. 229–241.

Mourad, A.-H.-I., El-Domiaty, A., Chao, Y.J., 2013. Fracture toughness prediction of low alloy steel as a function of specimen notch root radius and size constraints. Eng. Fract. Mech. 103, 79–93.

Mourad, A.H., Elsayed, H.F., Barton, D.C., Kenawy, M., Abdel-Latif, L.A., 2003. Ultra high molecular weight polyethylene deformation and fracture behaviour as a function of high strain rate and triaxial state of stress. Int. J. Fract. 120 (3), 501–515.

Mourad, A.H.I., Maiti, S.K., 1995. Influence of state of stress on mixed mode stable crack growth through D16AT aluminium alloy. Int. J. Fract. 72, 241–258.

Mourad, A.H., Maiti, S.K., 1996. Mode II stable crack growth. Fatigue Fract. Eng. Mater. Struct. 19 (1), 75–84.

Nasiri, S., Khosravani, M.R., 2023. Failure and fracture in polyethylene pipes: Overview, prediction methods, and challenges. Eng. Fail. Anal. 107496.

Nezbedová, E., Hutař, P., Zouhar, M., Knésl, Z., Sadílek, J., Náhlík, L., 2013. The applicability of the Pennsylvania Notch Test for a new generation of PE pipe grades [Article]. Polym. Test. 32 (1), 106–114. https://doi.org/10.1016/j.polymertesting.2012.09.009.

Nguyen, K.Q., Mwiseneza, C., Mohamed, K., Cousin, P., Robert, M., Benmokrane, B., 2021. Long-term testing methods for HDPE pipe-advantages and disadvantages: a review. Eng. Fract. Mech. 246, 107629.

Olamide, A., Bennecer, A., Kaczmarczyk, S., 2020. Finite Element Analysis of Fatigue in Offshore Pipelines with Internal and External Circumferential Cracks. Applied Mechanics 1 (4), 193–223.

Parmar, R., Bowman, J., 1989. Crack initiation and propagation paths for brittle failures in aligned and misaligned pipe butt fusion joints. Polym. Eng. Sci. 29 (19), 1396–1405.

Parmar, R. (1986). The long-term behaviour of butt fusion welds in polyethylene pipeline systems.

Parsons, M., Stepanov, E.V., Hiltner, A., Baer, E., 2000. Correlation of fatigue and creep slow crack growth in a medium density polyethylene pipe material [Article]. J. Mater. Sci. 35 (11), 2659–2674. https://doi.org/10.1023/A:1004789522642.

Pfeil, M.C., Kenner, V.H., Popelar, C.H., 1993. A fracture mechanics evaluation for the life expectancy of polyethylene butt fusion joints [Article]. Eng. Fract. Mech. 44 (1), 91–107. https://doi.org/10.1016/0013-7944(93)90084-6.

Plummer, C.J.G., Goldberg, A., Ghanem, A., 2001. Micromechanisms of slow crack growth in polyethylene under constant tensile loading [Article]. Polymer 42 (23), 9551–9564. https://doi.org/10.1016/S0032-3861(01)00476-1.

Popelar, S.F., Popelar, C.H., Kenner, V.H., 1991. Creep crack growth in joints of a thermoplastic [Article]. Int. J. Fract. 50 (2), 115–130. https://doi.org/10.1007/BF00035207.

Rahman, S., Brust, F.W., Ghadiali, N., Wilkowski, G.M., 1998. Crack-opening-area analyses for circumferential through-wall cracks in pipes—Part I: analytical models. Int. J. Press. Vessel. Pip. 75 (5), 357–373.

Robledo, N., Domínguez, C., García-Muñoz, R.A., 2017. Alternative accelerated and short-term methods for evaluating slow crack growth in polyethylene resins with high crack resistance [Article]. Polym. Test. 62, 366–372. https://doi.org/10.1016/j.polymertesting.2017.07.022.

Schoeffl, P.F., Lang, R.W., 2015. Effect of liquid oilfield-related media on slow crack growth behavior in polyethylene pipe grade materials [Article]. Int. J. Fatigue 72, 90–101. https://doi.org/10.1016/j.ijfatigue.2014.09.016.

Schouwenaars, R., Jacobo, V.H., Ramos, E., Ortiz, A., 2007. Slow crack growth and failure induced by manufacturing defects in HDPE-tubes [Article]. Eng. Fail. Anal. 14 (6 SPEC. ISS.), 1124–1134. https://doi.org/10.1016/j.engfailanal.2006.11.066.

Sehanobish, K., Botsis, J., Moet, A., Chudnovsky, A., 1986. An analysis for crack layer stability. Int. J. Fract. 32, 21–33.

Shaheer, M., Troughton, M., Khamsehnezhad, A., Song, J., 2017. A study of the micro-mechanical properties of butt fusion-welded joints in HDPE pipes using the nanoindentation technique. Welding in the World 61, 819–831.

Shahin, A., Barsoum, I., Islam, M.D., 2020. Constitutive model calibration of the time and temperature-dependent behavior of high density polyethylene [Article]. Polym. Test. 91, 106800 https://doi.org/10.1016/j.polymertesting.2020.106800.

Shi, J., Feng, Y., Tao, Y., Guo, W., Yao, R., Zheng, J., 2023. Evaluation of the seismic performance of butt-fusion joint in large diameter polyethylene pipelines by full-scale shaking table test. Nucl. Eng. Technol.

Soltaninezhad, S., Salavati, H., Goharrizi, A.S., 2019. Ductile fracture assessment of high-density polyethylene (HDPE-PE100) weakened by an inclined double keyhole notch. Theor. Appl. Fract. Mech. 104, 102349.

Stojimirovic, A., Kadota, K., Chudnovsky, A., 1992. An equilibrial process zone in polymeric materials [Article]. J. Appl. Polym. Sci. 46 (6), 1051–1056. https://doi.org/10.1002/app.1992.070460614.

Thuy, M., Niebergall, U., Oehler, H., Alig, I., Böhning, M., 2021. Evaluation of the damaging effect of crop protection formulations on high density polyethylene using the Full Notch Creep Test [Article]. Polymer 228, 123853. https://doi.org/10.1016/j.polymer.2021.123853.

TN-51 - Polyethylene Pipe Butt Fusion Structure, Process, and Terminology. (2018). In: Plastic Pipe Institute (PPI).

Trávníček, L., Poduška, J., Messiha, M., Arbeiter, F., Pinter, G., Náhlík, L., Hutař, P., 2023. Effect of recycled material on failure by slow crack growth in multi-layer polyethylene pipes. Eng. Fract. Mech. 109423.

Veselý, P., Kotter, I., Lach, R., Nezbedová, E., Knésl, Z., Hutař, P., & Grellmann, W. (2009). Prüfmethoden zur Analyse des lokalen mechanischen Verhaltens von Schweißnähten in Polyethylen-Kunststoffrohren. *Proc. Fortschritte der Kennwertenmittlung für Forschung und Praxis, December*, 3-4.

Wang, Y., Feng, G., Lin, N., Lan, H., Li, Q., Yao, D., Tang, J., 2023. A Review of Degradation and Life Prediction of Polyethylene. Appl. Sci. 13 (5), 3045.

Wee, J.W., Choi, B.H., 2016. Modeling of axisymmetric slow crack growth of high-density polyethylene with circular notched bar specimen using crack layer theory [Article]. Int. J. Solids Struct. 97_98, 189–199. https://doi.org/10.1016/j.ijsolstr.2016.07.030.

Wee, J.W., Choi, B.H., 2020. Stochastic study on effects of material and physical parameters on slow crack growth behaviors of HDPE using the crack layer theory [Article]. Int. J. Solids Struct. 195, 13–27. https://doi.org/10.1016/j.ijsolstr.2020.03.010.

Wee, J.W., Chudnovsky, A., Choi, B.H., 2020a. Discontinuous slow crack growth modeling of semi-elliptical surface crack in high density polyethylene using crack layer theory [Article]. Int. J. Solids Struct. 185–186, 65–77. https://doi.org/10.1016/j.ijsolstr.2019.08.016.

Wee, J.-W., Chudnovsky, A., Choi, B.-H., 2021. Crack layer model for semi-elliptical surface cracks in HDPE pipes and application in buried pipes with complicated loading conditions. Int. J. Mech. Sci. 106680.

Wee, J.-W., Chudnovsky, A., Choi, B.-H., 2023. Crack layer modeling of overload-induced slow crack growth retardation of high-density polyethylene. Int. J. Mech. Sci. 108546.

Wee, J.W., Park, S.Y., Choi, B.H., 2020b. Modeling and application of discontinuous slow crack growth behaviors of high-density polyethylene pipe with various geometries and loading conditions [Article]. Eng. Fract. Mech. 236, 107205 https://doi.org/10.1016/j.engfracmech.2020.107205.

Wu, X.-R., Xu, W., 2022. Weight function methods in fracture mechanics: Theory and Applications. Springer.

Xu, J., Zhang, Z.L., Østby, E., Nyhus, B., Sun, D.B., 2010. Constraint effect on the ductile crack growth resistance of circumferentially cracked pipes. Eng. Fract. Mech. 77 (4), 671–684.

Zerbst, U., Vormwald, M., Andersch, C., Mädler, K., Pfuff, M., 2005. The development of a damage tolerance concept for railway components and its demonstration for a railway axle. Eng. Fract. Mech. 72 (2), 209–239.

Zha, S., Lan, H.-Q., Huang, H., 2022. Review on lifetime predictions of polyethylene pipes: Limitations and trends. Int. J. Press. Vessel. Pip. 104663.

Zhang, H., Zhou, Z., Chudnovsky, A., 2014. Applying the crack-layer concept to modeling of slow crack growth in polyethylene. Int. J. Eng. Sci. 83, 42–56.